Stochastic finite elements analysis of large concrete structures' serviceability under thermo-hydro-mechanical loads – Case of nuclear containment buildings

D.E.-M. Bouhjiti, J. Baroth, F. Dufour, S. Michel-Ponnelle, B. Masson

Stochastic Finite Elements Analysis of large concrete structures' serviceability under Thermo-Hydro-Mechanical loads – Case of Nuclear Containment Buildings

D. E.-M. BOUHJITI[1,2,6,*], J. BAROTH[1,*], F. DUFOUR[1,3], S. MICHEL-PONNELLE[4] and B. MASSON[5]

[1]Univ. Grenoble Alpes, CNRS, Grenoble INP[†], 3SR, F-38000 Grenoble, France
julien.baroth@3sr-grenoble.fr
[2]Grenoble INP Partnership Foundation – Industrial chair PERENITI, Grenoble, France
david.bouhjiti@3sr-grenoble.fr
[3]PERENITI chairholder (EDF SEPTEN/DTG/CIH)
frederic.dufour@3sr-grenoble.fr
[4]Electricité De France (EDF-R&D), Paris, France
sylvie.michel-ponnelle@edf.fr
[5]Electricité De France (EDF-DIPNN-Technical Direction), Lyon, France
benoit.masson@edf.fr
[6]Currently in Egis Industries, Montreuil, TSA 50012-93188, France
david.bouhjiti@egis.fr

Abstract:

This work proposes a global Stochastic Finite Element Method (SFEM) to model the effects of concrete ageing uncertainties on the serviceability and durability of large reinforced and prestressed structures with a containment role. As their modelling requires strongly non-linear, coupled and expensive calculations with a large number of parameters, adapted and efficient probabilistic strategies need to be defined aiming at a stochastic analysis within a reasonable cost and a physically admissible representativeness. In this contribution, this is achieved through four steps: (a) the definition of a well-established physical framework based on a staggered Thermo-Hydro-Mechanical+Leakage (THM-L) model; (b) the limitation of random inputs for uncertainty propagation to the most influential ones using a variance-based Hierarchized and Local Sensitivity Analysis (HLSA); (c) the construction of a THM-L response metamodel using Polynomial Chaos Expansion (PCE); (d) the reliability analysis of serviceability criteria using Crude Monte Carlo Method (CMCM) applied to the developed metamodel. For validation purposes and demonstration of achievability within a complex industrial framework, this global methodology is applied to an experimental 1:3 scaled Containment Building of a nuclear reactor. Eventually, it is shown that a complete probabilistic analysis of a physically admissible total dry air leakage rate (indicative of a nuclear containment structure's performance) and its evolution in time are obtained within a computational time of tens of days only. Such result can provide insights and help during the decision-making process for the design, maintenance and risk assessment of large structures. For Nuclear Containment Buildings (NCB), a direct application would be the evaluation of lifespan extension based on a leakage-rate-defined criterion under operational loads.

Keywords: *THM-L metamodeling, Stochastic Finite Element Methods, uncertainty propagation, local and global sensitivity analyses, nuclear containment buildings.*

[*] Corresponding authors: david.bouhjiti@egis.fr / julien.baroth@3sr-grenoble.fr
[†] Institute of Engineering Univ. Grenoble Alpes

Acronyms

BC	Boundary conditions
CB	Containment Building
CEOS	French acronym for ‘’ Comportement et l’Evaluation des Ouvrages Spéciaux– fissuration, retrait ‘’ meaning ‘’ Behaviour and assessment of special structures – cracking and shrinkage ‘’
CMCM	Crude Monte Carlo Method
CV	Coefficient of Variation
DOE	Design-Of-Experiments
EA	Early Age phase
EAH	Equipment Access Hatch
EDF	Electricité De France
ENDE	French acronym for ‘’ Evaluation Non Destructives des Enceintes de confinement des centrales nucléaires ‘’ meaning ‘’ Non-destructive assessment of nuclear containment buildings ‘’
EvaDéOS	French acronym for ‘’ Evaluation non destructive pour la prédiction de la Dégradation des ouvrages et l’Optimisation de leur Suivi ‘’ meaning ‘’ Non-destructive performance assessment for the prediction of structures’ degradation and monitoring optimization ’’
FE	Finite Element
GSA	Global Sensitivity Analysis
HLSA	Hierarchized Local Sensitivity Analysis
LSA	Local Sensitivity Analysis
LT	Long Term phase
MCM	Monte Carlo Method
NCB	Nuclear Containment Building
OFAT	One-Factor-At-a-Time
OP	Operational Phase
PAH	Personnel Access Hatch
PCE	Polynomial Chaos Expansion
POP	Pre-Operational Phase
RF	Random Field
RH	Relative Humidity
RMSE	Root-Mean-Square-Error
RSV	Representative Structural Volume
SEL	Size Effect Law
SFEM	Stochastic Finite Element Methods
SR	Surface Response
SRM	Surface Response Methods
SV	Structural Volume
THM-L	Thermo-Hydro-Mechanical+Leakage
VeRCoRs	French acronym for ‘’ VErification Réaliste du COnfinement des RéacteurS ‘’ meaning ‘’ Realistic assessment of the nuclear reactors’ tightness ‘’
WIM	Weighted Integral Method

Symbols

$\dot{X} = \frac{\partial X}{\partial t}$	The derivative of the variable X over time
I_d	the identity tensor
$< X >_+ = \max(X; 0)$	A mathematical norm
$y(x_i^-);\ y(x_i^0);\ y(x_i^+)$	The response of a model y when the input x_i is at its minimal, mean and maximal value respectively whereas the rest of parameters $x_{j\neq i}$ are at their mean values
Q	The truncated polynomial order
$\{\psi_{\alpha\epsilon\mathbb{N}}\}$	The projection polynomial basis
Q	The maximal polynomial order of a multivariate polynomial basis $\{\psi_\alpha\}$
ξ_i	The normalized random quantity associated with the random input X_i
$\{a_\alpha\}$	A set of PCE coefficients
I_i^y	The contribution of a given parameter x_i to the total variance of an output y
$\hat{y}$	The metamodel approximation of a given model y
T	The time variable (s)

$T = T(\vec{x}, t)$	The temperature field (°C)
$\beta(T) = \int_{T_o}^{T} \rho_c\, C^p\,(r)\ dr$	The concrete's enthalpy (J/m^3)
ρ_c	The concrete's density (kg/m^3)
C^p	The concrete's thermal capacity (J/kg/°K)
λ_c	The concrete's thermal conductivity (J/s/m/°K)
Q_{th}	Macroscopic source term (J/m^3)
Q_∞	The volumetric hydration heat (J/m^3)
$\tilde{A}(\alpha) = \dot{\alpha}$	The chemical affinity associated with the hydration reaction
A	The normalized hydration rate
E_a^{th}	The apparent activation energy associated with the hydration process (J/mol)
R	The universal gas constant (8.314 J/°K/mol)
T_{ext}	The ambient temperature (°C)

$C_w = C_w(\vec{x}, t)$	The water content field (litre/m^3)
$C_{w,\alpha} = C_{w,\alpha}(\vec{x}, t)$	The water content at early age (litre/m^3)
$S_r = S_r(\vec{x}, t)$	The saturation rate field (%)
$C_{w,0}$	The initial water content in the concrete design mix (kg/m^3)
C	The cement content in the concrete design mix (kg/m^3)
D_w	The concrete's water diffusivity factor (m²/s)
(A_w, B_w)	Fitting parameters defining D_w according to the experimental results of water loss under controlled hydric environment
T_{ref}^W	The reference temperature at which the drying test is performed for (A_w, B_w) identification (°K)
E_a^W	The activation energy associated with the drying phenomena (J/mol)
RH_{ext}	The ambient Relative Humidity

ε_{TOT}	The total strain tensor
ε_{ELAS}	The damageable elastic strain
ε_{TH}	The thermal strain tensor
ε_{ES}	The endogenous shrinkage tensor
ε_{DS}	The drying shrinkage tensor
ε_{CR}	The creep strain tensor
ε_{CK}	The cracking strain
$w_{ck} = w_{ck}(\vec{x}, t)$	The crack opening field (m)
N_{ck}	The number of cracks per RSV
α_{th}	the coefficient of thermal expansion (/°K)
α_{ES}	the coefficient of endogenous shrinkage
α_{DS}	the coefficient of drying shrinkage
α_0	The percolation threshold defined as the hydration rate value from which the concrete starts developing its mechanical rigidity
R_t	The tensile strength (Pa)
E	The Young's modulus (Pa)
d	The damage variable
d_{EA}	The resultant damage variable at early age
$\boldsymbol{\sigma_{VE}}$	A stress tensor computed within a viscoelastic framework
h_{EF}	The characteristic size of a given FE
σ^{X}_{PREC}	The compressive load in concrete due to prestressing in the X principal direction (tangential or vertical) (Pa)
σ^{X}_{PRES}	The tensile load in concrete due to pressurization in the X principal direction (tangential or vertical) (Pa)
σ_{cable}	The tensile loads in steel prestressing cables (Pa)

k_{eq}	The equivalent permeability of concrete (m²)
Q_{flux}	A given volumetric air flow through a boundary Γ (m³/s)
Q_X	The total dry air leakage through a given SV $X \in \{GUSSET; WALL; EAH; DOME\}$ (normalized %)
Q_X^{RSV}	The total dry air leakage through a given RSV $X \in \{GUSSET; WALL; EAH; DOME\}$ (normalized %)
$Q_{total} = Q_{TOT}$	The total dry air leakage rate through the VeRCoRs structure (normalized %)
Q_{CRACK}	The total dry air leakage rate through the VeRCoRs structure's cracks (normalized %)
Q_{MASS}	The total dry air leakage rate through the VeRCoRs structure's mass (normalized %)
c_d	A fitting parameter defining the dependence of the permeability k_D on the saturation rate S_r
k_D	The permeability of concrete's mass using Darcy's formalism (m²)
$(\alpha'_d, \beta'_d, \alpha_d, \beta_d)$	Fitting parameters defining the effect of mechanical damage on the permeability k_D
(d_r, d_Y)	Strain-based variables defined to distinguish a reversible and irreversible parts of permeability due to damage
d_{lim}	A residual mechanical damage at full unloading which can be associated to an imperfect crack closure and the contribution of the microcracks' network around an existing macrocrack
δ	A fitting parameter to ensure the monotonousness of the equivalent permeability with the applied strain
μ_{air}	The dynamic viscosity of air (Pa.s)
β_k	The Klinkenberg coefficient (Pa)
k_F	The permeability of concrete's cracks using Poiseuille's formalism (m²)
ξ	A correction factor that cannot exceed one defining the effect of cracks' roughness and shape on the observed permeability k_F
$\Delta P_{air} = P_{air,1} - P_{air,2}$	The air pressure gradient between two edges of $P_{air,1}$and $P_{air,2}$ air pressure respectively (Pa)
$P_m = \frac{1}{2}(P_{air,1} + P_{air,2})$	The mean air pressure between two edges of $P_{air,1}$and $P_{air,2}$ air pressure respectively (Pa)

1. Introduction

Ageing of concrete in large and strategic civil engineering confinement structures (such as containment buildings, dams, basins, reservoirs, etc.) plays a major role with regards to their serviceability and durability. In the present framework, ageing of concrete refers principally to the hydration and maturity processes, the drying in an unsaturated environment, creep and cracking under simultaneous operational Thermo-Hydro-Mechanical (THM) loads (temperature less than 50°C, bulk relative humidity higher than 40%, compressive loads less than 30% of the compressive strength, tensile loads potentially exceeding the tensile strength); all together leading to a global loss of air tightness from the casting phases (early age) through the structures' lifespan (long term). As time advances, this affects their main role as containment structures and could lead to heavy and costly maintenance operations so as to maintain the respect of regulatory criteria and ensure a safe operational environment. Therefore, the prediction of concrete behaviour in time is a key topic for operators in order to accurately assess their structures' performance (ideally in real time), and, mostly, project its evolution over coming years for optimized maintenance scheduling.

To achieve such goal, and amongst existing solutions, FE modelling using Thermo-Hydro-Mechanical models with Leakage post-processing (THM-L) is generally performed. In most cases, the modelling stands within a deterministic framework [1][2][3][4] even though concrete properties and boundary conditions have been shown to have an intrinsic spatiotemporal variability [5][6]. The main difficulties to include such randomness in numerical models are related to three aspects:

- **THM-L model complexity:** The numerical simulation of concrete ageing requires the physical comprehension of all phenomena involved during its lifetime from the casting phase until the serviceability age limit. That should cover chemo-thermal [7], hydric [8], viscoelastic [9][10][11], size effect issues [12][13] and induced damage [14][15], hydraulic aspects [16][17]. As a result, concrete structures' simulation involves a large set of physical models showing naturally epistemic uncertainty and a large number of parameters intrinsically scattered at various scales [18][16][19]. Due to such complexity and uncertainty, the analytical derivation of those models cannot be achieved easily and the accurate prediction of concrete's local and global behaviours can only be done if uncertainties are included without altering the model's physical representativeness.
- **Partial knowledge of concrete properties and their randomness**: In most civil engineering applications, the quantification of concrete properties' spatial and aleatory variability is only partial. Therefore, even though numerical tools exist to simulate such randomness (for example by using discretized and FE-projected Random Fields [20] for each random property), the questions related to the measurement of spatial correlation lengths, correlation of inputs, coefficients of variation, distribution laws, ergodicity rule, etc. are, in most industrial cases, unanswered due to technological, time and cost limitations associated with the multi-scale experimental setups. In the absence of sufficient data, statistical analysis of inputs remains difficult and so is the quantification of uncertainty propagation through the THM-L structural response. Such issue can be alleviated (partially) if one refers to existing and relatively extensive experimental programs (VeRCoRs project [21], CEOS project [22], EvaDéOS project [23], ENDE project [24], decade long creep programs [25][26] as illustrative examples). One should keep in mind, though, that used concrete materials are not the same and the obtained conclusions are hardly generalizable to all concrete types and considered scales.
- **Limited calculation resources**: Deterministic THM-L models require a hefty computational time; especially when applied to full scale buildings (characteristic dimension of decametres). The first reason is related to the required refined mesh (characteristic size of centimetres) for objective localization modelling and the second is intrinsic to the physics as several equations require solving (thermal, hydric, mechanical and hydraulic) within a non-stationary framework and strong material-related and numerical non-linearities. As an order of magnitude, in the particular case of Nuclear Containment Buildings simulation, cumulative computational times vary from several hours to tens of days depending on whether cracks' localization occurs or not and on the complexity level of the used model [5][18][2]. When coupled to the use of Random Fields in order to introduce spatial variability of properties, the use of Monte Carlo Method seems unreasonable even in the presence of super-calculators and parallelization platforms; in particular for full-scale structures modelling [5][18]. This encourages the consideration for alternative methods which are less time consuming and more efficient.

This explains why in existing contributions (several examples are shown in Table 1), to the author's knowledge, stochastic modelling of concrete behaviour in large structures has been tackled only partially:

Table 1: Examples of partial and simplified stochastic analysis of concrete THM-L behavior in large structures

Reference (application)	Calculation Step (phase)	Model	Geometry - Model	Outputs	SA / PC
[27] (Roller-Compacted-Concrete dam)	T (early age)	Heat equation	2D-FE	Temperature Maturity	SA: RBD-FAST PC: RF+ MCM
[28] (general application)			3D-FE Hierarchal multi-scale		PC : LHS+ MCM
[29] (cracked wharves)	H (long term)		0D - Analytical	Lifespan based on chloride diffusion	PC: MCM
[30][31] (specimen scale)	H-L (long term)		0D - Analytical	Water content Saturation rate Permeability	SA: DOE
[32] (2x2x0.2 m^3 wall)			3D - FE		PC: RF+MCM
[33] (0.8x0.8x0.6 m^3 bi-axially prestressed wall)	M (long term) Bayesian updating framework	Non damageable viscoelastic model	3D-FE	Differed strains	SA/PC: MCM
[34] (general application)			0D - Analytical		PC: DFCM
[35] (Nuclear Containment Buildings)			1D-FE 0D - Analytical		PC: inverse FORM
[36] (general application)			3D-FE		PC: IS + SR (KLTE)
[37] (1.77x4.2x0.15 m3 shear wall)	M (long term)	Damageable viscoelastic model	3D-FE	Local (cracking patterns) and global (Force vs. displacement) responses	SA: OFAT PC: RF + MCM
[18] (Nuclear Containment Buildings)	M (early age + long term)	Damageable viscoelastic model	3D-FE	Local (cracking patterns) response	
[38][39] (Nuclear Containment Buildings)	M-L	Empirical damage-permeability law	0D - Analytical	Permeability / leakage rate	SA/PC : MCM

SA: Sensitivity Analysis – PC: Probabilistic Coupling – RF: Random Field – MCM: Monte Carlo Method – RBD-FAST: Random-Balance-Design FAST method – LHS: Latin Hypercube Sampling – DFCM: Density Forecast Combination Method – FORM: First Order Reliability Method – IS: Importance Sampling – SR: Surface Response – OFAT: One-Factor-At-a-Time – KLTE: Karhunen-Loève time expansion

- Focusing on one calculation step (T or H or M or L) or one ageing phase (early age or long term) without the others even though uncertainty propagation is expected to be non-negligible both from one THM-L calculation step to the other and over time.
- Using over-simplified geometries to model complex structural components; mainly 0D up to 2D approaches even though concrete's heterogeneity is 3D and so are the Boundary Conditions (BC), the stresses' and strains' spatial variability.
- Using some closed-form solutions to approximate the real response and facilitate the use of Crude Monte Carlo Methods. This might have the advantage of facilitating rapid simulations but leads to strong hypotheses as the material behaviour's non-linearity and the spatial variability of THM loads might be overlooked.

Though such attempts are worth exploring and are encouraged to some extent for engineering applications and to benchmark advanced stochastic methods, they remain highly questionable in terms of physical accuracy and representativeness of the real behaviour. Indeed, their used hypotheses include a non-negligible epistemic error that can be reduced through the consideration of an adapted and, mostly, full THM-L probabilistic modelling scheme; especially in the existence of uncertainty amplification from the specimen scale to the structural one and from the early age to the long term phase; all for a more inclusive risk assessment of concrete structures' serviceability and durability.

Accordingly, this contribution aims at enhancing the physical accuracy of concrete behaviour stochastic modelling:

- **In section 2:** A brief description of the global THM-L modelling strategy is provided. Its main hypotheses are recalled. In particular, highlighted aspects are related to the weak THM-L coupling and to the early-age and long term behaviours decoupling under practical and realistic loading configurations and boundary conditions.
- **In section 3:** Adapted sensitivity analysis and probabilistic coupling strategies are detailed based on the One-Factor-at-A-Time (OFAT) principle (for most influential parameters selection) and the Surface Response Modelling (SRM) theory (for meta-modelling and explicit description) respectively at low cost.
- **In section 4:** The relevance of the developed stochastic THM-L model framework is demonstrated based on experimental results (especially the dry air leakage estimation) for an experimental 1:3 scaled Containment Building in terms of (a) the description of the structural behaviour; (b) the selection of most influential parameters for uncertainty propagation at low cost; (c) the Surface Response (SR) construction at low cost and (d) the straightforward reliability analysis based on propagated uncertainties through the structure's lifespan.

2. Physical framework of concrete's dry air tightness simulation

The considered model hereafter corresponds to a staggered THM-L model that has been developed, defined and validated at both the specimen and structural scales in previous works [5][18][16] considering Nuclear Containment Buildings as an application. The aim of this section is to recall its main hypotheses and descriptive equations for forthcoming non-intrusive probabilistic coupling. The original model contains 63 parameters in total: 12, 9, 31, 11 for Thermal, Hydric, Mechanical and Leakage calculations respectively. However, for the sake of conciseness, only relevant physical and numerical parameters for the understanding of this paper are mentioned. Further details are provided in Appendix A.

2.1 Thermal calculations (T)

The first calculation step consists of solving the heat equation to simulate the time evolution of the concrete's temperature T. To account for hydration heat release at early age, an apparent and macroscopic source term Q_{th} is added [7] and Neumann boundary conditions are considered:

$$\dot{\beta}(T) - \nabla \cdot (\lambda_c \nabla T) = Q_{th} = Q_\infty \widetilde{A}(\alpha)\ e^{-\frac{E_a^{th}}{RT(t)}} \qquad \textbf{Eq. 1}$$

2.2 Hydric calculations (H)

The second calculation step consists of simulating the water content evolution in time due to hydration at early age and under drying fluxes during the operational phase. Calculations are performed in two phases:

- The first phase at early age where concrete hydration is undergoing and drying fluxes are prevented thanks to formwork and curing conditions (to favour the hydration process). One should note that, for thick structural elements, even if drying occurs during hydration, the coupling between water consumption by hydration and water loss by drying only concerns the first concrete layer and not the bulk volume. This is explained by the drying kinetic which is considerably slower than the one of hydration. Therefore, the hypothesis of hydration-drying decoupling remains valid for large structures even if

the curing conditions are not applied at early age [40][41][42]. Eventually, the water content evolution $C_w = C_{w,\alpha}$ in time is only due to the cement reaction with water and is modelled using the Powers and Brownyard model (for CEM I cement type) [43] relating linearly the water content decrease to the hydration rate α:

$$C_{w,\alpha} = C_{w,0} - 0.23 * c * \alpha \qquad \textbf{Eq. 2}$$

- The second step where the formwork and curing are removed exposing concrete edges to drying fluxes. The hydration process is supposed sufficiently advanced ($\alpha \to 1$) so as to neglect the water content changes due to hydration compared to the one due to hydric loads. So hydric calculations consist of solving the heat equation involving a non-linear and thermo-activated diffusivity factor D_w [44][45] and a desorption curve [46] relating the water content C_w (main unknown of the problem) and the relative humidity RH of concrete. As described in [44], Neumann hydric boundaries are expressed in terms of the relative humidity.

$$\dot{C_w} = \nabla \cdot (D_w \nabla C_w)$$
$$D_w(C_w, T) = A_w e^{B_w C_w} \frac{T}{T_{ref}^w} e^{-\frac{E_a^w}{R}\left(\frac{1}{T} - \frac{1}{T_{ref}^w}\right)} \qquad \textbf{Eq. 3}$$

2.3 Mechanical calculations (M)

The third step concerns the solving of the mechanical problem accounting for a damageable viscoelastic framework. The temperature and water content fields are used as inputs to define the induced strains such as endogenous, thermal and drying shrinkages and the effect on the viscoelastic behaviour of concrete. The total strain ε_{TOT} is divided into five main strains according to their origins (Eq. 4 – [18]).

Basic and drying creep calculations are performed using the Burgers model [18]. The dependence of each viscoelastic component on the hydration rate is defined according to the maturity method [47][48] and the Arrhenius' law is used to describe thermo-activation aspects [49]. As for concrete damage modelling, a strain-based, isotropic, unilateral, local [50] and energy-regularized [51] formulation is retained (Eq. 4). The contribution of creep to damage is computed based on a staggered creep-damage scheme [52][53] and the crack opening values are directly post-processed from the strain field using the strategy in [54].

$$\boldsymbol{\sigma} = (1 - d)\mathbf{E} : \boldsymbol{\varepsilon_{ELAS}}$$
$$\boldsymbol{\varepsilon_{TOT}} = \boldsymbol{\varepsilon_{ELAS}} + \boldsymbol{\varepsilon_{TH}} + \boldsymbol{\varepsilon_{ES}} + \boldsymbol{\varepsilon_{DS}} + \boldsymbol{\varepsilon_{CR}} \qquad \textbf{Eq. 4}$$
$$\boldsymbol{\varepsilon_{TH}} = \alpha_{TH}(T - T_0)\,\mathbf{I_d} \quad \boldsymbol{\varepsilon_{ES}} = \alpha_{ES} < \alpha - \alpha_0 >_+ \mathbf{I_d} \quad \boldsymbol{\varepsilon_{DS}} = \alpha_{DS}\left(C_w - C_{w,0}\right)\mathbf{I_d}$$

Finally, energetic and statistical size effects are accounted for using (a) a simplified '' Size Effect Law'' (SEL) relating the concrete's tensile strength R_t to its effectively stressed volume derived from the weakest link theory in [55] and (b) stationary and spatially correlated RFs [56][57] associated with the spatial variability of the Young's modulus E. Full details and physical gains of the coupling of RFs and SELs are detailed in [18]. The main advantage consists of defining a FE spatially variable behaviour law both before and after strain localization and during the propagation phase which leads to a realistic random description of the cracking pattern.

2.4 (air) Leakage calculations (L)

The fourth and last step allows the calculation, when needed, of the air permeability of concrete k_{eq} and the solving of the air transfer under imposed pressure gradient ΔP_{air}. This is done using a diffusion equation where the main unknown is the air pressure P_{air} within the concrete volume. The air flux Q_{flux} is integrated afterwards on the edge of interest Γ as following (derived from the Navier-Stokes' equation for a compressible fluid):

$$\dot{P_{air}} = \nabla \cdot \left(\frac{k_{eq}}{2\,\mu_{air}} \nabla \cdot P_{air}^2\right)$$
$$Q_{flux}(\Gamma) = \int_\Gamma -\frac{k_{eq}}{\mu_{air}} \nabla \cdot P_{air}\, d\Gamma \qquad \textbf{Eq. 5}$$

Two transfer modes for the equivalent permeability k_{eq} are usually considered for concrete depending on its mechanical state:

- The first mode refers to the concrete material as a homogeneous domain in terms of air transfer properties. Its permeability can therefore be described as an equivalent quantity representative of the volume's microstructural state. As damage increases, so does the connectivity and porosity of the porous network due to the deployment of microcracks. In the absence of strain localization, concrete is seen as a damage-dependent porous media which justifies the hypothesis of a transfer mode governed by Darcy's law k_D [58][59]. Hereafter, the effects of water content (saturation rate $S_r = \frac{C_w}{C_{w,0}}$) [60] ($f_1$ in Eq. 6), of pressure gradient (Klinkenberg effect) [61](f_2 in Eq. 6), of damage state are considered [16] distinguishing reversible and irreversible parts of permeability (f_3^r and f_3^i in Eq. 6).

$$k_D = k_0 \cdot f_1(S_r) \cdot f_2(P_{air}, S_r) \cdot \left(f_3^r(\varepsilon_{eq,t}) + f_3^i(\varepsilon_{eq,t})\right)$$

$$f_1(S_r) = \sqrt{1 - S_r}\left(1 - S_r^{\frac{1}{c_d}}\right)^{\frac{1}{2\,c_d}}$$

$$f_2(P_{air}, S_r) = 1 + (1 - S_r)\frac{\beta_k}{P_m} \qquad \textbf{Eq. 6}$$

$$f_3^r(\varepsilon_{eq,t}) = (\alpha'_d d_r)^{\beta'_d}\left(1 + \sum_{n=1}^{3}\frac{1}{n!}(\alpha_d\, d_r)^{n\,\beta_d}\right) \quad f_3^i(\varepsilon_{eq,t}) = \left(1 + \sum_{n=1}^{3}\frac{1}{n!}(\alpha_d\, d_\gamma)^{n\,\beta_d}\right)$$

- The second mode refers to the mechanical state where microcracks coalesce into macrocracks which are descriptive of a highly localized strain. The associated permeability k_F in that case is due to the fluid flow through the macrocrack openings w_{ck} and is commonly described using the Poiseuille's law (derivation of the Navier-Stokes' equations for perfectly parallel and infinite planes). The resultant macrocrack is supposed fully dry (though the hydric state of cracks in concrete is rarely studied) and the effects of the crack's shape and roughness on the air transfer properties are accounted for in a phenomenological way [62] using a correction factor ξ as follows:

$$k_F = \xi\frac{w_{ck}^3}{12\,h_{EF}}$$

$$\xi = \min\left((\alpha_w w_{ck})^{\beta_w}; 1\right) \qquad \textbf{Eq. 7}$$

As one can notice, the validity domains of k_D and k_F are distant in terms of the mechanical damage state; the first being used for microcracked volume and the second for macrocracked one. Accordingly, a continuous matching between the two modes is used based on a log-type matching law [16].

$$k_{eq} = (k_D)^{1-\left(\frac{<d_r - d_{lim}>_+}{1-d_{lim}}\right)^{\delta}} \cdot (k_F)^{\left(\frac{<d_r - d_{lim}>_+}{1-d_{lim}}\right)^{\delta}} \qquad \textbf{Eq. 8}$$

2.5 THM-L modelling strategy for large structures

Ideally, the here above described THM-L model can be used to simulate the whole structure's lifetime. However some model simplifications can be applied depending on the nature of the applied loadings and their evolution in time. In particular, for pre-stressed large concrete structures, the risk of cracking is more important at early age as the various strains due to the hydration process are restrained. Once the prestressing is applied, and if well designed, early age cracks are closed (at least partially) and new cracks (i.e., damage increase) are hardly obtained under operational loads [5]. As a consequence, and given those hypotheses, the decoupling of the early age phase (where a viscoelastic damageable framework is mandatory) and the long term operational phase (where a viscoelastic framework would suffice) is possible. The only condition is to account for early age damage state throughout the Operational Phase (OP) simulation. In terms of strain tensor $\boldsymbol{\varepsilon}^{\mathbf{OP}}$, cracking strain ε_{ck}^{OP} and crack opening w_{ck}^{OP}, this writes [6]:

$$\boldsymbol{\sigma}_{\mathbf{VE}}^{\mathbf{OP}} = (1 - d_{EA})\mathbf{E}:\boldsymbol{\varepsilon}^{\mathbf{OP}}$$

$$\varepsilon_{ck}^{OP} = \frac{d_{EA}}{1 - d_{EA}}\frac{\left|\left|\boldsymbol{\sigma}_{\mathbf{VE}}^{\mathbf{OP}}\right|\right|_+}{E} \qquad \textbf{Eq. 9}$$

$$w_{ck}^{OP} = h_{EF} \cdot \varepsilon_{ck}^{OP}$$

where d_{EA} is the damage value computed at early age using a damageable viscoelastic framework, $\boldsymbol{\sigma}_{\mathbf{VE}}$ is the viscoelastic stress tensor, $\boldsymbol{\varepsilon}^{\mathbf{OP}}$ is the resulting strain tensor, $\left|\left|\boldsymbol{\sigma}_{\mathbf{VE}}^{\mathbf{OP}}\right|\right|_{+}$ is the maximal principal tensile stress value (If positive, the crack opening is non-null. Otherwise, under compressive loads, macrocracks are supposed closed).

Eventually, the resulting global THM-L modelling strategy is depicted in Fig. 1.

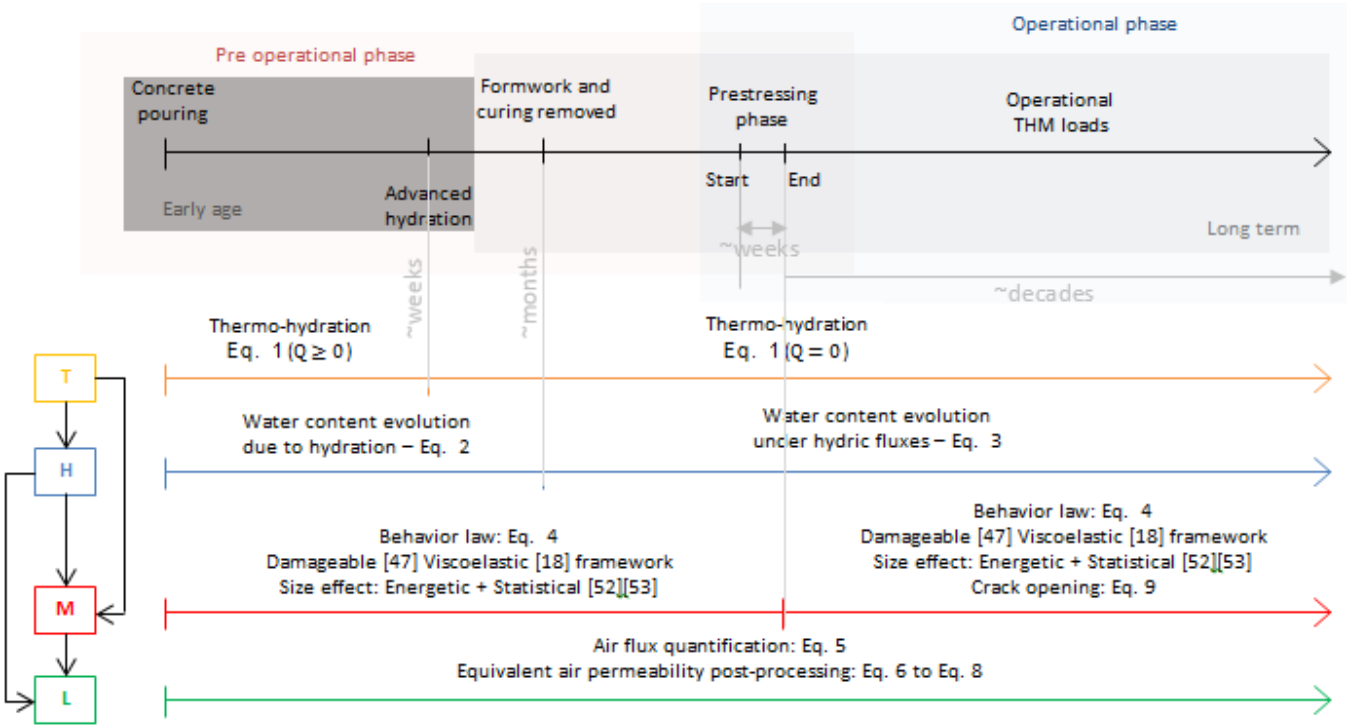

Fig. 1: Scheme of the global THM-L modelling strategy applied to large reinforced and prestressed concrete structures under simultaneous THM loads

3. Adapted stochastic strategies for THM-L uncertainty propagation

Given the important number of inputs (63 inputs in total: 12, 9, 31, 11 for Thermal, Hydric, Mechanical and Leakage calculations respectively – see appendix A) involved in the presented THM-L model and the non-linearity of concrete behaviour (thermo-hydration, creep, damage, permeability, etc.), the probabilistic analysis of structural behaviour using Crude Monte Carlo Method (CMCM) seems hardly achievable and practical. On the one hand, the consideration of all inputs as random remains highly questionable given that only a limited number (representative of physical phenomena) have a significant effect on the THM-L response's variation. In that sense, a prior sensitivity analysis is pertinent to identify the most influential parameters and phenomena and limit the number of random inputs for uncertainty propagation. On the other hand, the application of CMCM would require several calls of the THM-L model inducing hefty numerical cost.

One way to overcome such limitation is to approximate the FE models' response with an explicit Surface Response using a strategic and limited number of calculation points. Monte Carlo Method can, then, be applied at low cost to this explicit SR instead of the FE model. Obviously, the quality of the probabilistic analysis using the SR (referred to as surrogate model or metamodel) depends on the error gap between the FE model response and its approximation (metamodel). One should aim at low error given a certain computational time constraint and physical measurement precision.

Hereafter, a global stochastic approach for staggered THM-L modelling is detailed using Polynomial Chaos Expansion Method [63][64] where the most influential inputs are defined according to a prior 1st order, local and hierarchized OFAT-based [65][66] sensitivity analysis following the strategy depicted in Fig. 2.

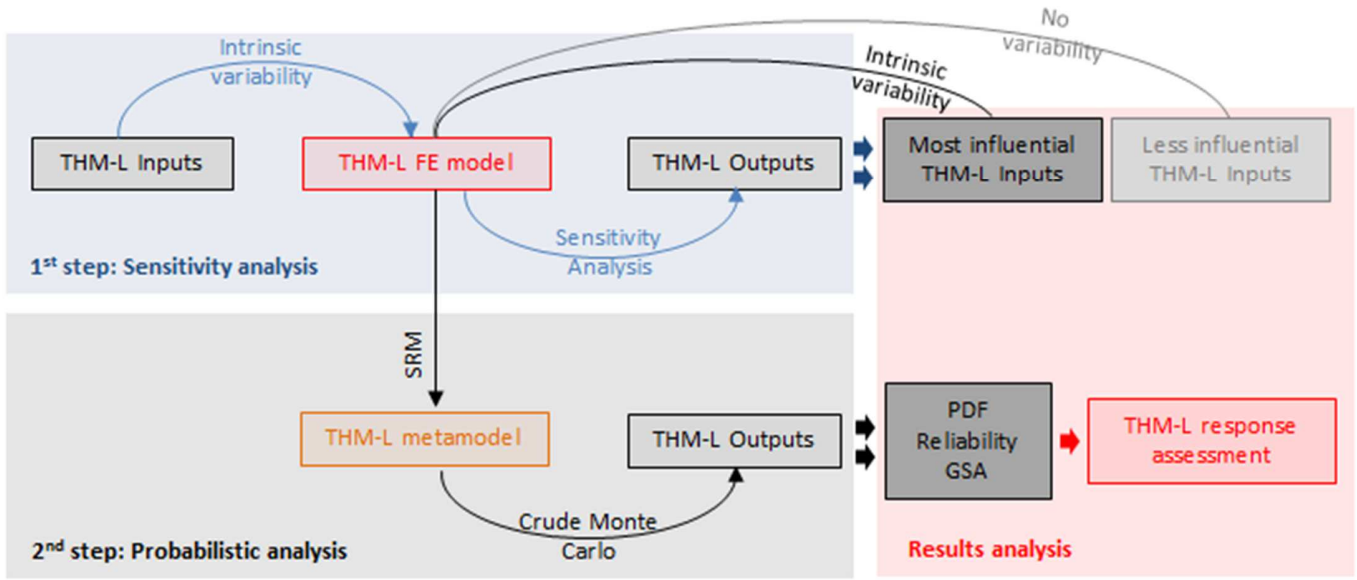

Fig. 2: Scheme of the global stochastic THM-L modelling strategy

3.1 Adapted sensitivity analysis strategy

The main goal of this part is to define an adapted sensitivity analysis strategy to cope with the high number of variable inputs and the high computational time of THM-L modelling. The priority is granted to the identification of the most influential parameters at the lowest cost possible without altering significantly the quality of the models' responses.

Accordingly, in this step, Global Sensitivity Analysis Methods (Monte Carlo Methods, Quadrature Methods, Spectral Methods, etc.) are by default discarded even though they ensure a precise quantitative description of models' sensitivity to the variation of their inputs (accounting for their respective probabilistic distributions). Indeed, their main drawbacks remain that they go beyond our sensitivity analysis purposes and aim at a full probabilistic coupling which is expensive when a high accuracy is looked for and when a high number of random inputs is considered even when adaptive schemes are used.

Therefore, our interest is geared towards Local Sensitivity Analysis Methods (LSAM) which are generally less expensive though less accurate in terms of statistical moments' quantification. Several methods exist in literature (perturbation method [67][68], Neumann method [69], the Weighted Integral Method (WIM) [70], Design-Of-Experiments (DOE) based methods [71][72][73][74]). Herein, and for practicality purposes, only non-intrusive strategies which are compatible with small and high perturbations are retained. In particular, One-Factor-at-A-Time (OFAT) methods offer the possibility of dealing with high number of inputs at lowest costs (Daniel's method [75], Cotter's method [66], Morris's method [76], Sobol's method [77]).

The simplest formulation consists of running, for each parameter, two simulations at its minimal and maximal boundaries whereas the rest of inputs are kept at their mean values [75]. Eventually, for N inputs, 2N+1 calculations are required (or N+1 if the model response shows some symmetry which is rarely the case for non-linear THM-L problems). Based on the obtained results, three results y are available per variable input $x_{i\epsilon[1,N]}$, one can approximate a mean response and also a variance estimate for a given coefficient of variation CV_i: $x_i^+ = (1 + CV_i)x_i^0$ and $x_i^- = (1 - CV_i)x_i^0$:

$$\mu_i^y = y(x_i^0) = \mu^y$$
$$\left(\sigma_i^y\right)^2 = Var[y(x_i^-);\ y(x_i^0);\ y(x_i^+)] \qquad \textbf{Eq. 10}$$

A qualitative order can then be derived based on the contribution of each input $x_{i\epsilon[1,N]}$ (assumed to be random) to the total variance of the model y as following:

$$I_i^y = \frac{\left(\sigma_i^y\right)^2}{\sum_{j=1}^{N}\left(\sigma_j^y\right)^2} \qquad \textbf{Eq. 11}$$
$$\sum_{i=1}^{N} I_i^y = 1$$

The classification of the I_i^y indicators allows the ordering of the various inputs based on their variance contribution and, by extension, based on the model sensitivity to their variations. One should define a certain criterion to judge whether a parameter is influential or not. For instance one can consider all first inputs that contribute to at least 80% of the global variance as influents. Being a LSAM, one should note that its results are merely qualitative and their representativeness should be verified afterwards by performing a GSA using the obtained reduced list of inputs.

The default application of such methodology to THM-L calculations would require:

- $2*n_T$ +1=25 Thermal calculations (for n_T =12 thermal inputs) when interested in the thermal outputs (temperature and hydration rate)
- $2*(n_T + n_H)$ +1=43 Hydric calculations (for n_T =12 thermal and n_H =9 hydric inputs) when interested in the hydric outputs (water content, saturation rate, relative humidity)
- $2*(n_T + n_H + n_M)$ +1=105 Mechanical calculations (for n_T =12 thermal, n_H =9 hydric and n_M =31 mechanical inputs) when interested in the mechanical outputs (strains, cracking patterns, stresses, prestressing losses)
- $2*(n_T + n_H + n_M + n_L)$ +1=127 Leakage calculations (for n_T =12 thermal, n_H =9 hydric, n_M =31 mechanical and n_L =11 leakage inputs) when interested in the leakage rate outputs (permeability, air leakage rate)

However, as some parameters are expected to be significantly more influential than others, only most influential inputs should be retained along the THM-L sensitivity analysis path. That means that, for instance, for the Hydric model sensitivity analysis only most influential Thermal inputs need to be included along with all the hydric parameters. The same goes for the

mechanical and leakage calculations where only most influential TH and THM inputs should be considered respectively. For cost reduction, this selective sensitivity analysis should be applied from one calculation step to the other but also in time when moving from the early age phase towards the long term one. Being an adaptive approach, cost reduction cannot be foreseen in advance as it depends on the obtained SA results and the contribution of each input to the global variance at each step.

The global strategy for such Hierarchized and Local Sensitivity Analysis (HLSA) from the early age phase to the long term one is depicted in Fig. 3.

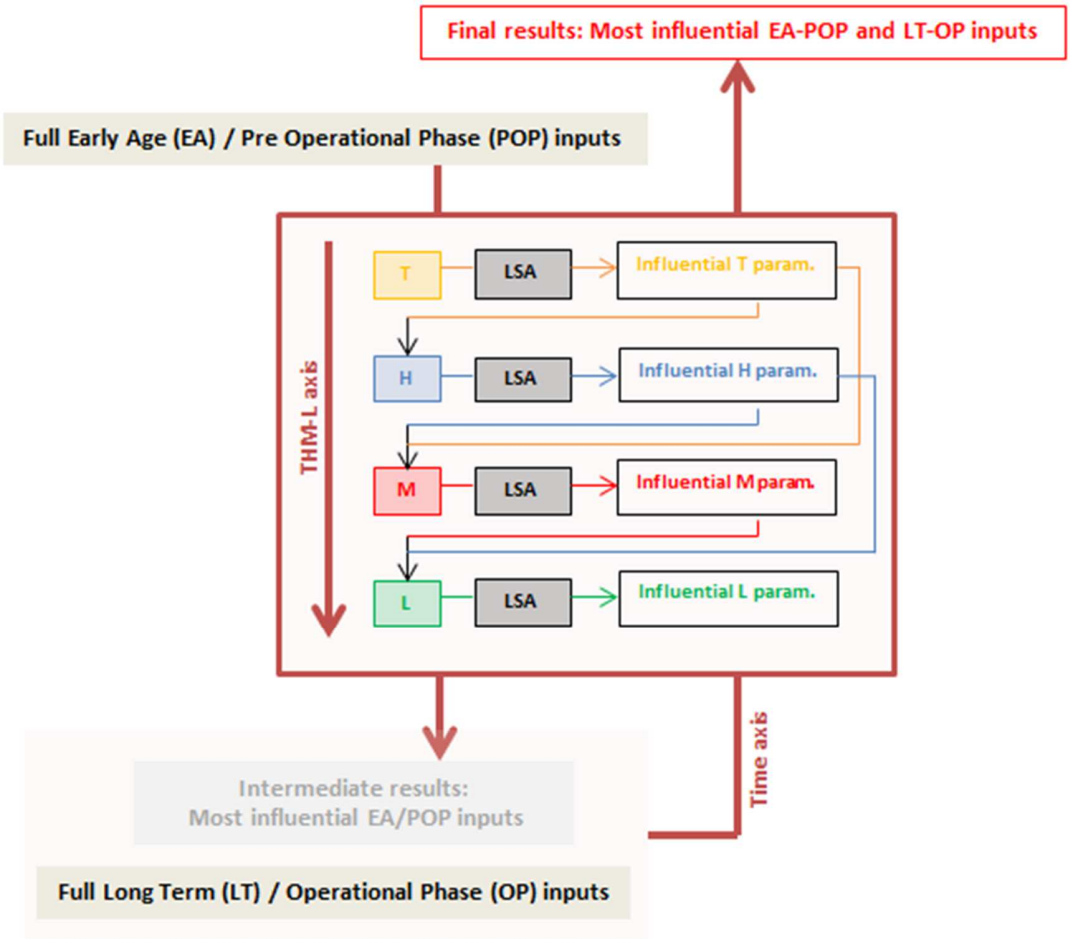

Fig. 3: Scheme of the HLSA applied to staggered THM-L calculations

3.2 Adapted probabilistic and reliability analyses strategy

After the reduction of the list of random inputs to the most influential ones, the aim of this part is to perform a full probabilistic description of the THM-L behaviour of concrete at a reasonable cost.

By default, Monte Carlo Methods which are theoretically applicable to all physical problems regardless of their complexity are discarded. Indeed, for a failure probability of $10^{2-\log_{10} N}$, N random sampling is required to achieve a slow convergence rate $o\left(1/\sqrt{N_{sample}}\right)$ and $o\left(1/N_{sample}\right)$ for Monte Carlo and quasi-Monte Carlo Methods respectively. Also, probabilistic methods limited to the tail distributions (FORM/SORM reliability analysis methods, etc.) are overlooked since they do not allow a quantification of the first statistical moments nor the computation of the whole distribution function.

On the contrary, our interest is geared towards Spectral Methods which aim at fitting the model's response to an explicit and finite development (polynomial [64] or other [63]) using a limited/optimized number of model call (regression methods [78], projection methods [79][80], adaptive methods [81][82]) and a given approximation error before applying Crude Monte Carlo Methods for a probabilistic description and adequate Global Sensitive Analysis (GSA) in a fast-forward way [83][84].

In particular, the Polynomial Chaos Expansion (PCE) methodology is of interest herein [63] under the hypotheses of independent random inputs and orthonormal polynomial basis of the associated Hilbertian space. In this work, the integration points of each input are, by default, defined using the classical Gauss-Quadrature Method (projection method) (More mathematical details are provided in the appendix B). One should note that other adaptive schemes could be applied for more cost optimization but this is considered out of the scope of the present paper as a reference study is needed first.

Eventually each model y depending on a certain number P of inputs $x_{i\epsilon[1,P]}$ can be approached in a polynomial way:

$$y(x) \approx \hat{y}(x) = \sum_{\alpha=0}^{Q<+\infty} y_\alpha \Psi_\alpha(X) \qquad \textbf{Eq. 12}$$

The truncating order Q is to be selected based on computational time [85] or error-related criteria ($||y - \hat{y}||$, $\left||\mu_y - \mu_{\hat{y}}|\right|$, $\left||\sigma_y^2 - \sigma_{\hat{y}}^2|\right|$) [82]. Once the explicit metamodel $\hat{y}$ is constructed and its approximation of the real response y considered valid and accurate, Crude Monte Carlo can be performed at low cost which facilitates the post-processing of the statistical moments, the sensitivity analysis indexes and the failure probabilities to a certain threshold.

4. Application to Nuclear Containment Buildings – case of the VeRCoRs mock-up

The above global THM-L stochastic modelling strategy is applied in this section to the behaviour of concrete in Nuclear Containment Buildings (NCBs); particularly to the case of an experimental 1:3 double walled containment building mock-up monitored by EDF company named VeRCoRs [21]. For the sake of conciseness, in-depth results analyses are limited herein to the air leakage rate (final calculation step of interest). Other intermediate THM results (temperature at early age, water content, delayed strains, etc.) are briefly shown and analysed for the sake of illustration.

4.1 Overview

NCBs ensure two main roles. The first one is structural allowing bearing some dead and active loads of static or dynamic nature related to operational and accidental situations (protection from external aggressions). And the second, of interest in this work, is rather functional to ensure the protection of the environment from radioactive matter under operational loads or in the case of a nuclear accident. In the case of double walled NCBs (Fig. 4a-e), such tightness is ensured by the inner wall made out of reinforced and prestressed concrete (Fig. 4a, c, f – Fig. 5). Accordingly, the concrete aging leads to a global loss of tightness which needs to be maintained to a certain regulatory threshold to allow a safe working environment. In France, operators, under the control of the Nuclear Safety Agency, and for full scale NCBs, have to demonstrate once every decade that their buildings tightness ensures a leakage rate lower than 1.5% of the total gas mass inside the inner building per day under a pressure difference of 4.2 bars between the inner and outer side of the wall. Additional safety margins are applied by EDF to account for the concrete aging during the decade after the test, leading to an operational threshold of 1.125% of the total gas mass inside the inner building per day.

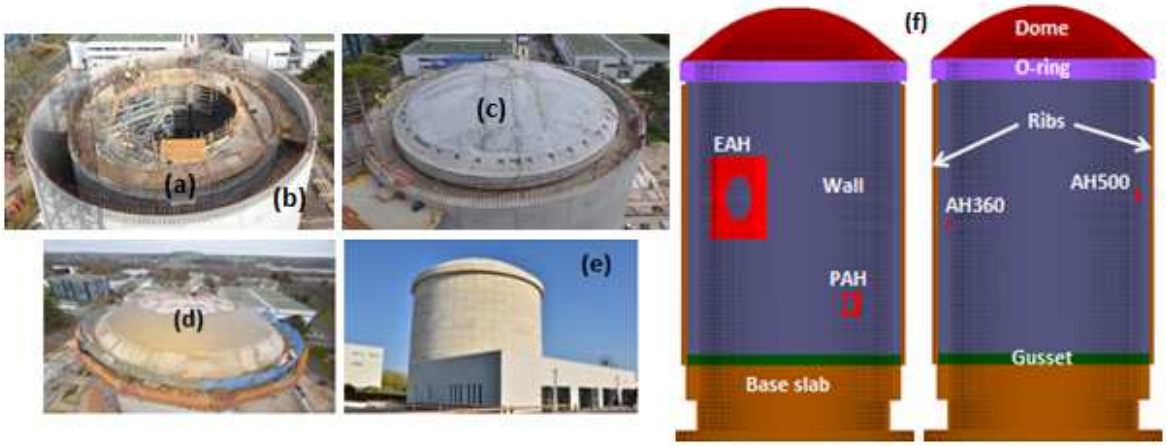

Fig. 4: Experimental 1:3 scaled double-walled NCB – VeRCoRS mock-up (a) Inner wall (b) Outer wall (c) Inner dome (d) Outer dome (e) Full mock-up (f) Schematic drawing of the inner wall's structural parts

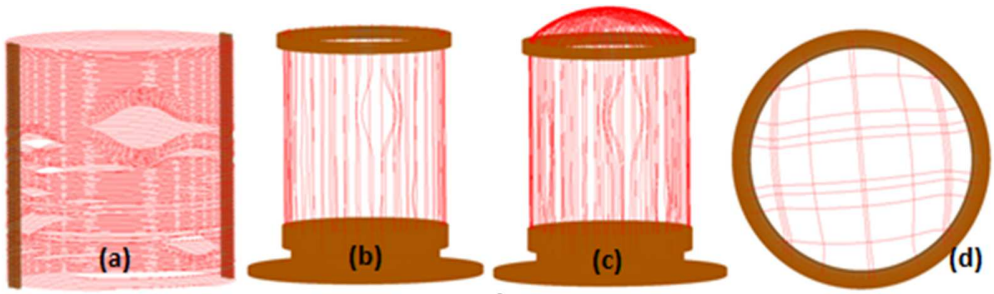

Fig. 5: Types of prestressing cables in NCBs (a) Horizontal cables limited to the wall's height (b) Vertical cables limited to the wall's height (c) Gamma cables crossing the wall and the dome (d) Dome cables

In France, the initial design lifespan for NCBs was set at 40 operational years. However, given the good performance of some NCB's up to this day, the extension of their lifespan to +60 years is now considered. For that reason, EDF has launched a considerable evaluation and maintenance program to assess the actual state of its nuclear fleet and engage necessary reparations for the lifespan extension within a safe environment. Amongst those efforts, the VeRCoRs program which consists of studying the ageing of an experimental 1:3 scaled containment building under realistic operational THM loads. Given the scale reduction, the ageing of the mock-up is expected to be faster than the one of a full scale building. In terms of drying, and given the same concrete type, the 60-year ageing period is expected to be reduced 9 times for the VeRCoRs structure [21]. Also, in terms of dry air permeability criterion, the previous thresholds should be multiplied by 3^2 (due to volumetric scale reduction) and become 13.5% and 10.1% respectively. One should note that such scale effect concerns only the regulatory criterion and not the air leakage rate value through the inner wall.

Generally speaking, the loss of structural air tightness is due to several things; amongst which there are:

- Early-age cracking: the hydration of concrete is accompanied with thermally and chemically induced (shrinkage mostly) strains showing naturally a gradient in the concrete thickness. If restrained, especially for new lifts in the presence of a hardened and thicker old one, they lead to the development of early age cracks which increases locally the permeability of the structure and reduces its global tightness. An example of the cracking pattern in the VeRCoRs mock-up is depicted in Fig. 6 for the particular case of the gusset area (1st lift of the NCB following the base slab). As the restraining mainly occurs in the tangential direction (due to the closed ring effect), the main patterns consist of vertical cracks which are observed from both sides of the wall (inner and outer sides). However, their paths through the wall are hardly known though the hypothesis of vertical through cracks is generally made. In addition, one can note that the distribution of these cracks is not correlated to the positions of singular parts (hatches and ribs for example); but rather linked to the (heterogeneous) restrained effect applied by the base slab.
- Drying: Drying leads to the reduction of concrete's saturation rate and therefore increases its air permeability which in turn decreases the global tightness as well, given the important exposed area of the containment wall.
- Prestressing losses: Even though prestressing is achieved thanks to post-tensioned and cement grouted cables (Fig. 5) aiming at a residual compressive load of 1 MPa under 4.2 bars relative air pressure (for a 40-year based design period), and due to structural rigidity heterogeneousness, the risk of tensile stresses development is non-null in certain structural elements (especially in the principal tangential direction associated with a cylindrical coordinates' system). It might be the case right after tensioning phase or later on in time as concrete creep and drying lead to a loss in prestressing for constant tensile pressurization loads. In the presence of early-age cracks, their re-opening is problematic as they become active and highly increase the leakage rate of the structure.

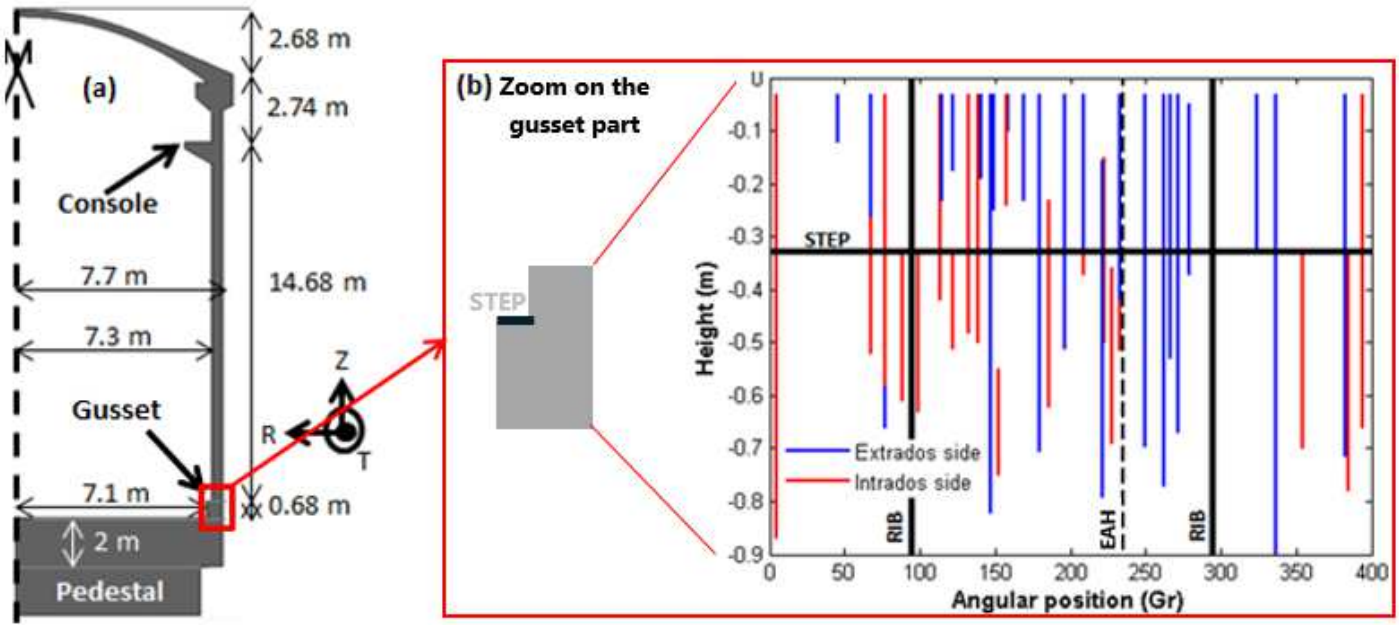

Fig. 6: (a) 2D-Axis view of the VeRCoRs inner wall (b) In situ observations of the cracks' distribution at the gusset level from the intrados and extrados sides at 12 days after casting (400 **Gr** = 360 angular degrees)

The foreseen experimental program is the following:

Table 2: Relevant dates of the VeRCoRs research program [21]

Phase name		Dates (inner wall)	Monitored inner temperature
Construction phase		24.07.2014 - 19.03.2015	Inner temperature = Ambient air temperature (~15°C)
Prestressing phase		16.05.2015 - 13.08.2015	
Operational phase	Pressurization Test 0	05.11.2015	
	Pressurization Test 1	25.01.2016*	
	Pressurization Test 2	15.03.2017	Continuously heated inner temperature (~35°C) (Heating is stopped during the pressurization tests only)
	Pressurization Test 3	21.03.2017	
	Pressurization Test 4	27.03.2018**	
	Pressurization Test 5	2020	
	Pressurization Test 6	2021***	
	Pressurization Test 7		
	Pressurization Test 8		

*07.03.2016 (1st benchmark) **27.08.2018 (2nd benchmark) ***2021 (3rd and last benchmark)

Using the previously defined THM-L stochastic strategy, a prediction of the evolution of air leakage rate (pressurization tests 0 to 8 in Table 2) in time is undertaken hereafter with an immediate interest in defining the risk of exceeding the regulatory values and foreseeing the time of maintenance according to a certain defined probability of failure.

4.2 The FE model

To allow sufficiently refined analysis of both local and global behaviours of the VeRCoRs mock-up's inner wall, and secondarily to limit the computational time, a Representative Structural Volume (RSV) strategy is retained herein [5][18][19]. Three conditions are used to define those RSVs (a) geometrical representativeness in terms of geometrical symmetries; (b) structural representativeness in terms of loads and boundary symmetries and (c) material representativeness in terms of spatial scattering and local behaviour simulation (strain localisation and multi-cracking in particular). Accordingly, the VeRCoRs inner wall is decomposed into 4 Structural Volumes (SV): the gusset, the wall, the EAH and the dome. The remaining structural volumes (PAH, the ribs, etc.) are overlooked in this analysis as their effect on the global THM-L response and their contribution to the total air leakage rate remains negligible. Then, each SV is decomposed into several RSVs which dimensions are shown in Fig. 7. Given this scale reduction, the finite elements characteristic size is reduced to 6-7 cm even though the structural dimension remains of decametres. This also allows an accurate simulation of passive rebars and active cables using 1D finite elements and assuming a perfect concrete-steel bond.

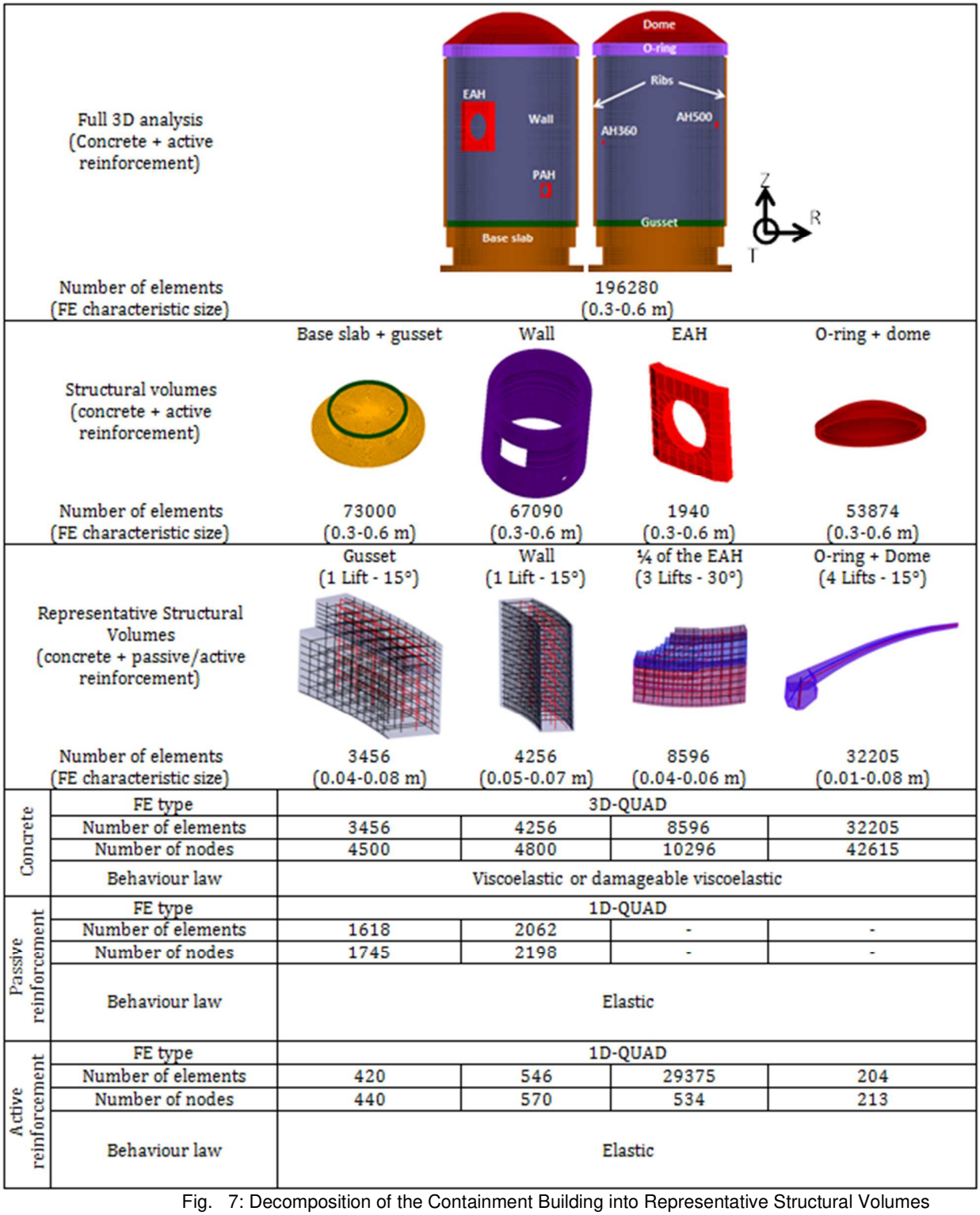

Concrete	FE type	3D-QUAD			
	Number of elements	3456	4256	8596	32205
	Number of nodes	4500	4800	10296	42615
	Behaviour law	Viscoelastic or damageable viscoelastic			
Passive reinforcement	FE type	1D-QUAD			
	Number of elements	1618	2062	-	-
	Number of nodes	1745	2198	-	-
	Behaviour law	Elastic			
Active reinforcement	FE type	1D-QUAD			
	Number of elements	420	546	29375	204
	Number of nodes	440	570	534	213
	Behaviour law	Elastic			

Fig. 7: Decomposition of the Containment Building into Representative Structural Volumes

In terms of the total air leakage rate, the full structure's leakage rate Q_{total} is simply obtained by superposing all RSV's contributions (the gusset's Q_{GUSSET}^{RSV}, the wall's Q_{WALL}^{RSV}, the EAH's Q_{EAH}^{RSV} and the dome's Q_{DOME}^{RSV}). For the particular case of the VeRCoRs structure, and given the RSV's geometries provided here above, this writes:

$$Q_{total} = Q_{GUSSET} + Q_{WALL} + Q_{EAH} + Q_{DOME}$$
$$\begin{cases} Q_{GUSSET} = 24 * Q_{GUSSET}^{RSV} \\ Q_{WALL} = 268 * Q_{WALL}^{RSV} \\ Q_{EAH} = 4 * Q_{EAH}^{RSV} \\ Q_{DOME} = 24 * Q_{DOME}^{RSV} \end{cases} \quad \textbf{Eq. 13}$$

In terms of boundary conditions, temperature and relative humidity profiles are directly issued from in situ measurements and are, when needed, extrapolated based on the projected operational loads defined by EDF [21]. They are directly applied to inner and outer surfaces of the RSVs using Neumann boundary conditions. For the mechanical boundaries (Fig. 9):

- At early age, simulations cover two lifts (the newly casted one and the old hardened one) to properly predict the cracking patterns. The upper surface of the new lift is free until the next lift is casted. From that point on, a uniform vertical displacement is assumed. For the lateral edges, axisymmetric boundaries are applied throughout the analysis.
- For the long term phase, simulations cover only the newly casted lift with identical boundaries. Concrete prestressing σ_{PREC} is applied indirectly by tensioning the cables at a certain level σ_{cable} and accounting for instantaneous losses based on the BPEL99 recommendations (those losses include the elastic shortage, frictions, the anchorage seating and also the differed effect of steel relaxation‡ – see appendix C [5]). As for delayed losses, they are computed implicitly as following:

$$\sigma_{cable}(t) = \sigma_{cable}(t_0) + E_a(\boldsymbol{\varepsilon_{CR}}(t - t_0) + \boldsymbol{\varepsilon_{DS}}(t - t_0)) \cdot \mathbf{n} \quad \textbf{Eq. 14}$$

Where $\sigma_{cable}(t)$ is the prestressing load in the cable, $\sigma_{cable}(t_0)$ the prestressing load after removing the instantaneous losses, E_a the cable Young's modulus and $\boldsymbol{n}$ a unitary vector associated with the cable direction.

Finally, to simulate the effect of the pressurized dry air on the containment building (Fig. 8), equivalent lateral and vertical tensile pressurization loads σ_{PRES} are directly applied on the lateral and upper surfaces of RSVs respectively.

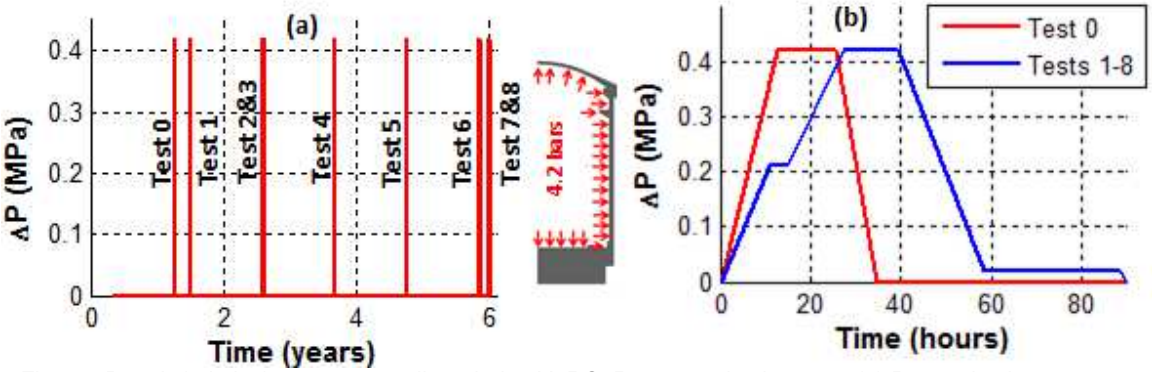

Fig. 8: Dry air (relative) pressure gradient during VeRCoRs pressurization tests (a) Pressurization tests program (b) Evolution of air pressure in time per test

‡ Based on the regulatory formula in appendix C, the relaxation losses in the VeRCoRs mock-up reach 56% after 1 year and more than 77% after 2 years only.

<table>
<tr><td rowspan="2">Stage for each lift
t_0: base slab casting
$t_{0,i}$: i^{th} lift casting</td><td colspan="4">Boundary conditions</td></tr>
<tr><td>Thermal</td><td>Hydric</td><td>Mechanical</td><td>Leakage</td></tr>
<tr><td>Hardening phase
(~ $t_{0,i}$+28 days)</td><td> 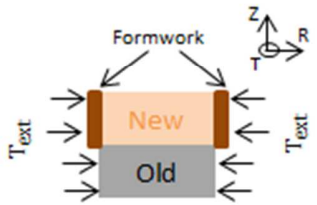
</td><td>No external drying</td><td> 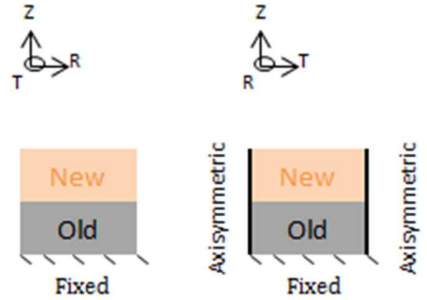
</td><td rowspan="2">No pressure gradient</td></tr>
<tr><td>Formwork removal
Next lifts casting
(~ $t_{0,i}$+ 2 weeks)

Prestressing phase
(~ t_0 + 1 year)</td><td rowspan="2"> 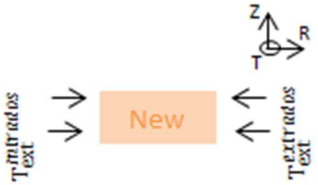
</td><td rowspan="2"> 
</td><td rowspan="2"> 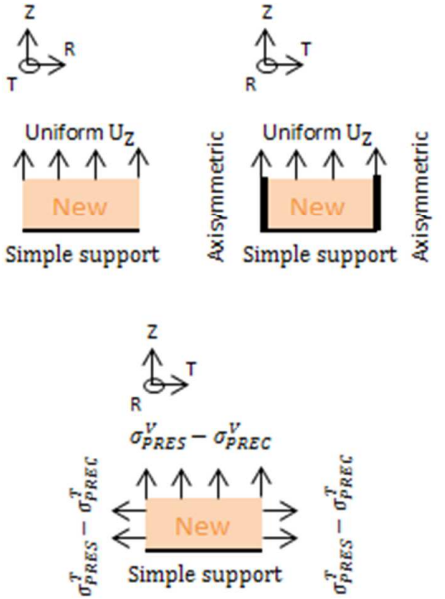
</td></tr>
<tr><td>Pressurization phase
(Fig. 9)</td><td> 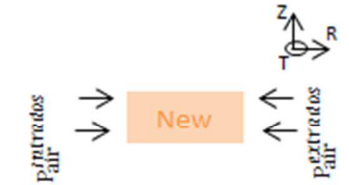
</td></tr>
</table>

Fig. 9: Summary of the Boundary conditions applied on the VeRCoRs RSV's (2D views of a 3D RSV associated with a cylindrical coordinate system in Fig. 6a and Fig. 7)

4.3 THM-L sensitivity analysis

The performed sensitivity analysis covers all 63 inputs in appendix A, using the strategy defined in section 3.1. The coefficients of variation associated with each input have been defined based on:

- in situ observations when the available sampling is considered representative
- based on previous works for a similar concrete types in the absence of sufficient experimental data,
- based on experts' judgement in the absence of experimental data and sufficient literature references. Practically, this is the case of some leakage model inputs (in appendix A) which have been investigated (in the cited references [16][21][59][62]) for a different concrete type but not as extensively as needed to have accurate estimation of each input's variation. So, such inputs are considered highly uncertain (with regards to the VeRCoRs concrete knowledge) and their coefficient of variation is deliberately overestimated (conservative approach compared to the variation observed in [16][21][59][62]).

Details about each coefficient of variation and the way it has been defined are provided in appendix A. In this part, the aim is to show the results of such sensitivity analysis, the cost reduction due to its hierarchal implementation through the THM-L steps and from the early age to the long term one. A preview of the obtained results is provided hereafter (Fig. 10).

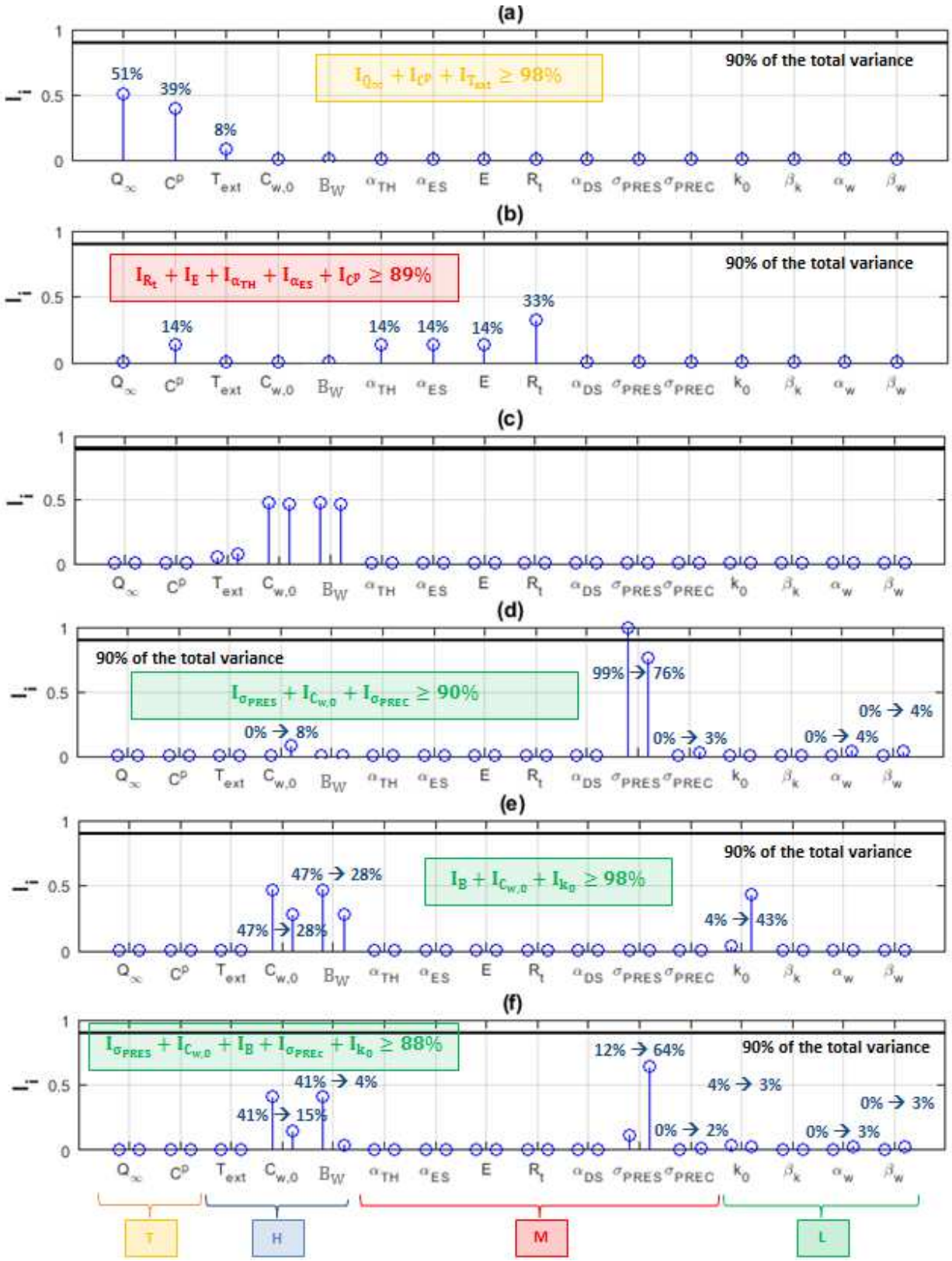

Fig. 10: Contribution of the most influential inputs to the global variance (in a local sense – section 3.1) of (a) the peak temperature at early age in the gusset; (b) the number of cracks per gusset's RSV; (c) the mean saturation rate in the wall at 1 and 6 years; (d) the leakage rate through the gusset's cracks during 1st and last pressurization tests; (e) the leakage rate through the VeRCoRs mass during 1st and last pressurization tests and (f) the total leakage rate through VeRCoRs mock-up during 1st and last pressurization tests.

4.3.1 Thermal calculations (T)

12 inputs have been considered initially leading to 25 thermal calculations. Taking the case of the gusset in Fig. 4 (60 cm thick element), and considering the output (scalar variable) ''Peak temperature at early age'' which is representative of the cracking risk at early age, the contribution of each input to the global variance in the sense of Eq. 11 is quantified (Fig. 10a). Eventually, only two parameters are retained as they contribute by more than 90% to the global variance: the hydration heat Q_∞ and the thermal capacity C^p in Eq. 1. For the long term phase, operational temperatures at the inner $T_{ext}^{intrados}$ and outer $T_{ext}^{extrados}$ sides of the wall are retained as they affect the most the resultant temperature profile (their contribution to the total variance of the temperature in the wall's thickness exceeds 99% - this is expected in the absence of external heat term and stationary regime mode solving). So for the remaining HM-L sensitivity analysis, only 3 parameters are retained: 2 at early age (Q_∞, C^p) and 1 for the long term phase (T_{ext}) in addition to all HM-L inputs.

4.3.2 Hydric calculations (H)

9 parameters have been considered initially in addition to most influential Thermal parameters. Here the case of the wall in Fig. 4 (40 cm thick element) is considered (Fig. 10c). At early age, and considering the ''water content decrease rate'' (time-dependent scalar variable) as the output of interest, two parameters seem to affect mostly the hydric response: the initial water content $C_{w,0}$ in the mix and the hydration heat Q_∞ (given the thermo-activation, this value affects the overall hydration kinetic). When considering the ''water content at the end of the early age phase'' (scalar variable) as an output of interest, the total response variance is defined by the one of the initial water content according to Eq. 2 with $\alpha = 1$. For the long term phase, the variance of the water content (time-dependant scalar variable) variable is defined up to 90% by the initial water content $C_{w,0}$ and the parameter B_w in the diffusivity factor D_w in Eq. 3. Over time, and as the water content drops, the model sensitivity to the variation of B_w and $C_{w,0}$ slightly decreases. Such results underline the importance of water to cement ratio in the design mix and its effect on the long term drying response of large structures. It also shows how the diffusivity factor is an important parameter in the prediction of the hydric state of concrete and its evolution in time. So for the remaining M-L sensitivity analysis, only 3 thermal parameters (Q_∞, C^p, T_{ext}) and 2 Hydric ones ($C_{w,0}B_w$,) are retained in addition to M-L inputs.

4.3.3 Mechanical calculations (M)

31 parameters have been considered initially in addition to the most influential TH parameters. At early age, the considered variable of interest, having ultimately an influence in the leakage rate through damages areas, is the '' cracking pattern '' of concrete and mainly the number of cracks per RSV (scalar variable). Here the example of the gusset is explored (Fig. 10b) (one should note that numerically the cracking risk for other RSVs remains negligible). As influential parameters, and as expected qualitatively, one finds: the tensile strength, the Young's modulus and their spatial scattering showing an important effect on concrete cracking (they contribute by more than 47% to the global variance). A lesser effect is shown by the thermal α_{TH} and shrinkage α_{ES} coefficients (contribution to the global variance limited to 14% each) of which the strains are restrained and by the hydration heat Q_∞ and thermal capacity C^p affecting the peak temperature and thermal shrinkage at early age.

For the long term phase, and considering the ''ultimate prestressing losses '' as the output of interest (which is representative of the risk of early-age cracks reopening under pressurization loads), influential parameters are the residual prestressing loads $\sigma_{PREC}^T - \sigma_{PRES}^T$ (in the tangential direction mainly as cracks are vertical), initial water content $C_{w,0}$, diffusivity factor B_w, and the drying shrinkage coefficient α_{DS} (their contribution to the global variance is of 42%, 33%, 05% and 15% respectively). One should note that, for all RSVs, no new cracks (other than the early age ones) under pressurisation loads are obtained for the considered coefficients of variation in appendix A.

Eventually, and based on those results, all ageing phenomena are identified (thermo-hydration, early age cracking, drying, prestressing losses) and parameters associated with them as well. So for the remaining L sensitivity analysis, only 1 thermal parameter (C^p), 2 Hydric ones ($C_{w,0}$, B_w) and 7 mechanical ones (R_t, E, α_{TH}, α_{ES}, α_{DS}, σ_{PREC}, σ_{PRES}) are retained in addition to L inputs.

4.3.4 Leakage calculations (L)

11 parameters have been considered initially in addition to the most influential THM parameters. In this part, the whole VeRCoRs structure is analysed (Eq. 13) according to three air leakage modes:

- ''the leakage rate through early-age cracks '' (Fig. 10d): As mentioned previously, early age cracks might reopen during the operational phase depending on the residual prestressing state under pressurization loads. If closed ($\sigma_{PRES}^{T} - \sigma_{PREC}^{T} \leq 0$), the air flow through cracks is at its lowest values. However, the leakage value can increase enormously if the same cracks reopen ($\sigma_{PRES}^{T} - \sigma_{PREC}^{T} > 0$). This importance of the residual stress in concrete is demonstrated by the used HLSA as it shows that it contributes by more than 75% to the total variance of the leakage through cracks. Parameters affecting concrete cracking at early age show relatively less influence since they only influence the number of cracks not their opening values. Over time and as crack opening values increase, the residual prestressing shows a decreasing influence compared to other parameters directly linked to prestressing losses under drying fluxes (water content $C_{w,0}$) and to the roughness and shape effects of cracks (α_w, β_w in Eq. 7 – their influence on the air leakage increases with the crack opening values). One should also note that, given our sensitivity analysis results, it has been shown that :
  - the peak air flow rate through cracks during the pressurization tests is not dependent on the Darcy's flow mode
  - the resulting cracking patterns do not show interferences between early cracks which remain independent air-flow-wise. Experimentally, cracking patterns might show some connectivity between cracks due to the existence of defects, inclusions or porous casting joints (this is not covered in our modelling).
  - cracks at early age show sensibly the same early age damage value d_{EA} regardless of their number per RSV. As a consequence, their opening values during the operational phase are identical.

So, the superposition principle remains applicable when several cracks are obtained per RSV; in other words, for the same THM-L inputs, the leakage rate through a RSV with N cracks is equal to N times the leakage through the same RSV with one crack (Eq. 15).

$$Q_{GUSSET}^{RSV}(N_{ck}\ \text{cracks}) = N_{ck} * Q_{GUSSET}^{RSV}(1\ \text{crack}) \qquad \textbf{Eq. 15}$$

- ''the leakage rate through concrete's mass'' (Fig. 10e): As expected, air tightness of concrete is shown to be strongly influenced by concrete drying phenomena (contributing initially by more than 94% to the global variance) represented by the initial water content variable ($C_{w,0}$) and the diffusivity parameter (B_w). As time advances, and the concrete's saturation level drops ($f_1(S_r) \rightarrow 1$ in Eq. 6), the model sensitivity to the intrinsic permeability k_0 increases considerably (up to 43%) compared to the contributions of $C_{w,0}$ and B_w (28% each).
- ''the total leakage rate'' (Fig. 10f): Considering the total air leakage rate (through early age cracks and through the concrete's mass which are demonstrated to be superposable numerically), and as concrete aging is not advanced, parameters affecting the total leakage rate are mainly of hydric nature (i.e., the water content $C_{w,0}$ and the diffusivity parameter B_w with an initial contribution to the total variance exceeding 80%). The sensitivity of the model to the residual prestressing loads variation (affecting the air flow through cracks) is relatively less (partial variance of 12%). As time advances, the water content decreases and the prestressing losses increase allowing higher crack opening values, the influence of the residual prestresses becomes non negligible (partial variance exceeding 60%) compared to the one of hydric inputs (dropping to a partial variance of 19%). This also informs about (a) the importance of the air leakage increase through cracks (when present) compared to the one through concrete's mass especially for the long term operational phase and (b) the criticality of early age damage in large concrete structures and its effect on the long term operational lifespan.

4.3.5 HLSA conclusions

Eventually, by considering the suggested HLSA and with regards to the total air leakage rate sensitivity to the various THM-L inputs variation, the following results are obtained[§]:

[§] In terms of computational cost, and using 14 node core (i7-7700HQ processor / Quad-Core 2.8 GHz-3.8 GHz Turbo), one Thermal simulation lasts 20 minutes per RSV, one Hydric simulation lasts 20 minutes per RSV, 1 mechanical simulation lasts

- From the 63 inputs, only 9 are shown to be really influential ($C_{w,0}$, B_w, R_t, E, α_{TH}, α_{ES}, σ_{PRES}, σ_{PREC}, k_0) given the coefficients of variation in appendix A. Those inputs are depicted in Fig. 11.
- By using the HLSA from one calculation step/phase to the other, the number of calculations (per RSV in Fig. 7 and compared to the default OFAT-based LSA) has decreased by:

- 0% for Thermal analysis (T): Being an initial step, all 12 Thermal inputs have been considered. So the number of simulations remains 25.
- 40% for Hydric calculations (H): In addition to the 9 Hydric inputs, only 3 influential thermal parameters have been considered instead of 12. So the number of hydric calculations drops from 43 to 25.

between 4 and 20 hours (depending on the damage state at early age) per RSV and 1 leakage simulation lasts 20 minutes per RSV.

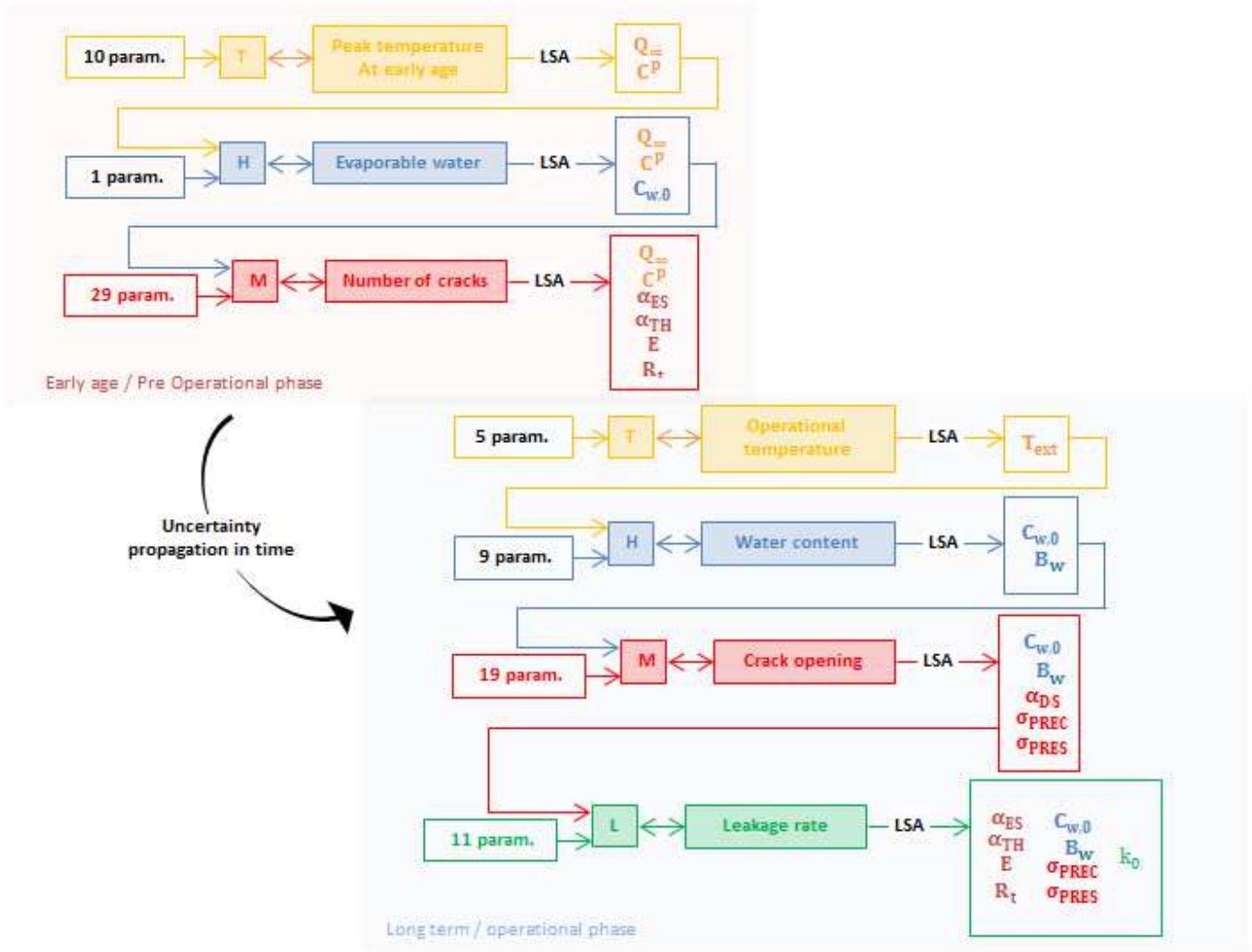

Fig. 11: Application of the OFAT-based HLSA to the THM-L calculations

- 15% for Mechanical calculations (M): In addition to the 31 mechanical inputs, only 3 Thermal inputs and 2 Hydric ones are included in the SA. Accounting for the decoupling between early-age and long term phases, the number of simulations goes down from 127 to 107.
- 66% for the Leakage calculations (L): In addition to the 11 leakage inputs, only 7 mechanical, 2 hydric and 1 thermal inputs are considered. So the number of leakage simulations drops to 43 instead of 127.

- As early age cracks concern only the gusset, the computation of the leakage rate through cracks is limited to the gusset RSV. This means that, when aiming at the distribution of the total air leakage rate, stochastic THM-L calculations are required for the gusset RSV whereas only stochastic H-L calculations are needed for the rest of RSVs. Accordingly, the identification of the total leakage rate can be simplified into a sum of the air flow through cracks (concerning the gusset only) and the one through the concrete's mass as shown in Eq. 16.

$$\begin{aligned} Q_{total} &= Q_{CRACK} + Q_{MASS} \\ Q_{CRACK} &= 24 * N_{ck} * Q_{GUSSET}^{RSV}(1\ crack) \\ Q_{MASS} &= 24 * Q_{GUSSET}^{RSV}(0\ cracks) + 268 * Q_{WALL}^{RSV} + 4 * Q_{EAH}^{RSV} + 24 * Q_{DOME}^{RSV} \end{aligned} \qquad \textbf{Eq. 16}$$

One should keep in mind that, in terms of the computed variances, the obtained results using the HLSA should be looked at in a qualitative way (in terms of relative tendencies and evolution in time for a given parameter compared to the others). For a more precise quantitative description of the various outputs' variance a GSA is undertaken hereafter.

4.4 THM-L metamodel and probabilistic/reliability analysis

In this part, the main focus is geared towards the long term aging of concrete and its effect on the total air tightness of the VeRCoRs structure. The list of the retained parameters and their random distributions are detailed in Table 3.

Table 3: Random distributions of most influential THM-L inputs and outputs of interest

Inputs →		POP		OP		POP				OP				Number param.	3rd order PCE terms	Effective cost per RSV With EA cracks (Without EA cracks)	Root-Mean-Square-Error (RMSE) Maximal value over time	Coef. of determination
		Q_∞	C^P	B_w	$C_{w,0}$	E	R_t	α_{ES}	α_{TH}	α_{DS}	σ^T_{PREC}	σ^T_{PRES}	k_0					
Mean		82	880	0.05	132	36	4.5	70	10	7.1	0.5	0.8	$2.7\ 10^{-17}$					
Unit		$\frac{MJ}{m^3}$	$\frac{J}{kg\ °K}$	-	$\frac{litre}{m^3}$	GPa	MPa	$\frac{\mu m}{m}$	$\frac{\mu m}{m\ °K}$	$\frac{\frac{\mu m}{m}}{\frac{litre}{m^3}}$	MPa	MPa	m^2					
CV		40%	40%	20%	20%	10%	10%	10%	10%	10%	50%	50%	50%					
PDF		Log[1]	Log[1]	Log[1]	Log[1]	Log[2]	Log[2]	Log[1]	Log[1]	Log[1]	Log[3]	Log[3]	Log[3]					
Outputs ↓																		
POP	Temperature	X	X											2	10	16 Thermal 16 Thermal	3°C	0.99
	Strains		X			X	X	X	X					5	56	1024 Mechanical EA 0 Mechanical EA	5 µm/m	0.95
OP	Relative Humidity			X	X									2	10	16 Hydric 16 Hydric	1.5%	0.99
	Strains			X	X					X	X	X		5	56	1024 Mechanical LT 1024 Mechanical LT	68 µm/m	0.98
	Crack openings			X	X						X	X		4	35	256 Mechanical LT 256 Mechanical LT	16 µm/m	0.99
	Flow through cracks			X	X	X	X	X	X		X	X		8	165	1280 Leakage (0 Leakage)	2.13%	0.91
	Flow through mass			X	X								X	3	20	64 Leakage (64 Leakage)	1.10%	0.98
	Total air flow			X	X	X	X	X	X		X	X	X	9	220	-	-	-

[1]Experts' judgment following the principle of maximum entropy [86] [2]From an experimental set of data at the specimen scale [3] From an experimental set of data at the structural scale

For a given quantity depending on N random and independent parameters, and for a given maximal order of the polynomials $\text{order}(\psi_\alpha) \leq q$ (in Eq. 12), the number of polynomial terms is of $Q = \frac{(N+q)!}{N!q!} - 1$. Using the Gauss-Quadrature Method (projection method), this would require $(q+1)^N$ calculations. In the present contribution, and to establish a reference analysis, the order of polynomial terms ψ_α is limited to q=3 arbitrarily as recommended in [85]. Of course, further analysis is required to define the relationship between the order of the polynomials, the error between the metamodel and actual model's response and the computational cost. This work however remains out of the scope of the present paper where the aim is to define and set a global stochastic approach before aiming at further computational or methodological optimization (in addition to the ones established in section 4.3.5).

Eventually, the computational cost for each quantity of interest in Table 3 is deduced (accounting for model simplifications in section 4.3.5). In the particular case of the total air leakage rate, and using a 3rd order polynomial, the foreseen PCE writes**:

$$Q_{TOT} \approx \widehat{Q_{TOT}} = \sum_{\alpha=0}^{219} a_\alpha \, \psi_\alpha\left(\xi = \left\{\xi_{B_w}, \xi_{C_{w,0}}, \xi_E, \xi_{R_t}, \xi_{\alpha_{ES}}, \xi_{\alpha_{TH}}, \xi_{\sigma_{PRES}}, \xi_{\sigma_{PREC}}, \xi_{k_0}\right\}\right) \quad \text{Eq. 17}$$

$$\xi_i = \frac{\log(X_i) - \mu_{\log,i}}{\sigma_{\log,i}} \text{ and } P_i \equiv \text{Hermite}; X_i \in \left\{B_w; C_{w,0}; E; R_t; \alpha_{ES}; \alpha_{TH}; \sigma_{PREC}; \sigma_{PRES}; k_0\right\}$$

where ξ_i is the normalized random quantity associated with the random input X_i, $\{a_\alpha\}$ a set of PCE coefficients, $(\mu_{\log,i}, \sigma_{\log,i})$ the mean and standard variation of the quantity $\log(X_i)$ following a normal law, ψ_α a multivariate Hermite polynomial term.

4.4.1 Discussion about the PCE metamodel accuracy

Using a 3rd order PCE, and based on the obtained Root-Mean-Square-Error (RMSE) of the metamodel and the actual FE responses, the various quantities of interest in Table 3 are approximated in a satisfactory way:

- In the case of the principal strains (tangential and vertical) at early age, the maximal RMSE value over time is of 5 µm/m which is considerably less than the in-situ measuring precision (uncertainties associated with strain gauges are of 10 µm/m).
- The PCE approximation is less satisfactory for the long term principal strains as the RMSE (at the end of VeRCoRs's lifespan) is of 68 µm/m. However, one should note that, though unknown, the long term measuring precision is expected to be higher than 10 µm/m due to the ageing of measuring devices and the eventual loss of adherence with concrete.
- For the crack opening values, the error (RMSE of 16 µm) is way less than the one of the crackmeters used on site (precision of 100 µm) but higher than the one of optical fibres (precision of 1 µm). However, it is important to underline the complexity of measuring the crack opening values on site as their positions are not known a priori and are hard to identify a posteriori.
- Finally, in terms of the leakage rate, expressed in the portion of air volume exiting the wall during the pressurization tests under normalized temperature and pressure, the obtained RMSEs are of 2.1% and 1.1% for the flow through early age cracks and through concrete mass respectively. Though not known precisely, the uncertainties associated with the in-situ measuring of the air leakage rate are believed to be higher than those values (given the technical difficulty of locating and accessing defects on site and the uncertainties related to used measuring techniques [87]).

Based on this analysis, the 3rd PCE order seems satisfactory in the absence of further and more precise measures of uncertainties on site. In all cases, the improvement of the metamodel accuracy is conditioned by two things: (a) the proper quantification of uncertainties on site to define the precision values to aim at and (b) the increase of the polynomial orders aiming at such precision.

** In terms of computational cost, the evaluation of the 220 polynomial terms requires 11 months using 14 node core (i7-7700HQ processor / Quad-Core 2.8 GHz-3.8 GHz Turbo). However, by using 10 parallel nodes - which is the case herein -, such cost is reduced to 34 days only.

4.4.2 GSA vs. HLSA analysis

In terms of tendencies, the GSA (Fig. 12) shows the same results as the previous HLSA. However, in terms of the computed variances, the GSA provides more insight on the importance of each input given its associated distribution:

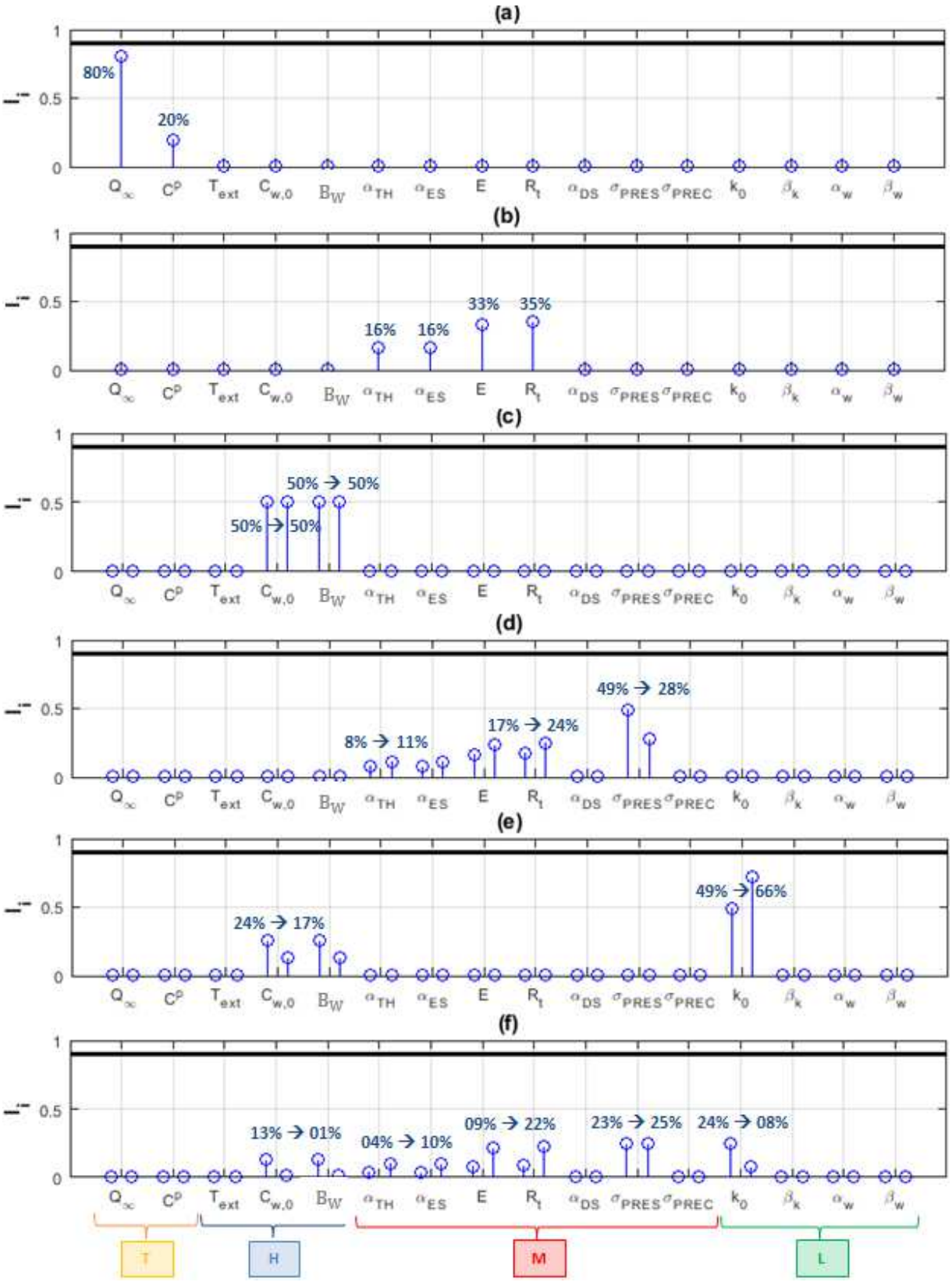

Fig. 12: Total Sobol' indexes (variance based GSA) for (a) the peak temperature at early age in the gusset; (b) the number of cracks per gusset's RSV; (c) the mean saturation rate in the wall at 1 and 6 years respectively; (d) the leakage rate through the gusset's cracks during 1st and last pressurization tests respectively; (e) the leakage rate through the VeRCoRs mass during 1st and last pressurization tests respectively and (f) the total leakage rate through VeRCoRs mock-up during 1st and last pressurization tests respectively

- For the thermal response (Fig. 12a), the peak temperature at early age shows more sensitivity to the hydration heat Q_∞ than to the thermal capacity C^p variation. Unlike the HLSA results, where both parameters have almost equal influence on the total variance, the GSA shows that, given the distribution of each, Q_∞ contributes 4 times more to the total variance than C^p.
- For the cracking response (Fig. 12b), the number of cracks per RSV is more sensitive to the variation of the tensile strength R_t and the Young's modulus E than to the one of the thermal expansion α_{TH} and endogenous shrinkage α_{ES} coefficients. Though the same conclusions were derived using the HLSA, one can notice that the GSA shows higher effect of E – close to the one of R_t –. This result makes more sense as both E and R_t define the strain damage threshold and the risk of exceeding it. Also, one can note that the contribution of R_t and E is twice as much than the one of α_{ES} and α_{TH} to the total variance of early age cracks.
- For the hydric response (Fig. 12c), the GSA shows the initial water content $C_{w,0}$ and the diffusivity factor B_w equally influential over time strengthening the fact that both drive the drying of concrete under hydric fluxes.
- For the air flow:

- Through cracks (Fig. 12d), as shown by the HLSA, the importance of the residual tensile stresses $\sigma^T_{PRES} - \sigma^T_{PREC}$ (in the principal tangential direction) is maintained with regards to the reopening of early age cracks and increasing the global structural permeability. The same goes for the decrease of its contribution to the global variance over time due to ageing phenomena (from 50% to 30%). However, unlike HLSA results, more importance is shown for the early age parameters (especially R_t and E with an equal contribution increasing from 17% to 24%) defining the number of cracks rather than the drying phenomena ($C_{w,0}$, B_w). This does not forcibly contradict the HLSA results – which remains qualitatively valid –. It rather adds further information as it underlines the non-negligible effect of the early age phase on the delayed behaviour of such large structures.
- Through the concrete mass (Fig. 12e), the GSA confirms (a) the increase of the contribution of the ''intrinsic'' permeability k_0 to the total variance and (b) the equal decrease of the one of drying parameters ($C_{w,0}$, B_w) over time due to water loss. However, quantitatively, the performed GSA shows a higher contribution (compared to HLSA results) to the total variance for k_0 (with values varying from 50% to 66%) and lesser and equal contributions for $C_{w,0}$, B_w inputs.
- Through the structure (Fig. 12f), and as shown by HLSA, as drying is not advanced, the parameters affecting the leakage rate's variance are of hydric nature ($C_{w,0}$; B_w) in addition to a higher (twice as much) contribution of k_0 (all totalling a contribution of 50%). The remaining 50% are shared by parameters defining (a) the number of cracks at early age (27%) and (b) their operational opening values (23%). As time advances, the importance of air flow through cracks becomes more critical. Accordingly, the GSA shows an increase of the effect of the residual tensile stresses and of the number of early age cracks (contributing to the total variance by up to 90%). On the other hand, the effects of hydric inputs and the intrinsic permeability become less influential (dropping to a 10% contribution).

Eventually, based on the performed GSA and with regards to the total air leakage rate sensitivity to the various THM-L inputs variation, the following results are obtained:

- Qualitatively, the HLSA and GSA show similar results. This can be seen as an *a posteriori* validation of the suggested HLSA as an efficient approach to achieve inputs selection and dimensional reduction before performing advanced THM-L SA and probabilistic coupling.
- The variance of the structural tightness of the VeRCoRs mock-up, and given the used distributions in Table 3, is due by (1st test: 26% → 9th test: 64%) to the variance of the cracking response at early age, by (1st test: 23% → 9th test: 25%) to the operational loads', by (1st test: 50% → 9th test: 10%) to the hydric/hydraulic properties'.

4.4.3 Probabilistic and reliability analysis

The application of Direct Monte Carlo Method (DMCM) to the PCE-based metamodels allows direct access to the Cumulative Density Functions (CDF) of the various outputs of interest (preview of available results expressed in CVs are provided in Table 4).

Table 4: Coefficients of variation associated with the various inputs of interest

			CV		
			NUM		EXP
Phase →			POP	OP (from Test 0 to Test 8)	
Outputs of interest ↓					
Gusset	Peak temperature at early age		13 %		10 %***
	Cracks' spacing per SV		101 %		111 %
	Delayed strains	Tangential		32 %*	27 %***
		Vertical		50 %*	66 %***
	Mean crack opening			90 % → 45 %**	
	RH			11 % → 9 %**	
VeRCoRs	Leakage rate	Through cracks		173 % → 136 %**	Not Available
		Through mass		168 % → 66 %**	
		Total		163% → 133 %**	

* quasi-constant over time during the operational phase ** Evolution between the 1st and last pressurization tests *** Data acquired from 24 strain gauges and 24 thermal sensors positioned at the gusset's intrados and extrados within a cover distance of 5 cm.

In the particular case of the air leakage rate through the VeRCoRs mock-up, the obtained results are depicted in Fig. 13 for the air flow rate through concrete mass, through early age cracks and through the whole structure. One should note that, at the stage of this study, available results are limited for the first 4 pressurization tests (Test 0 to 3) corresponding to the first 3 years of the operational lifespan of the VeRCoRs mock-up (2015-2018). Additional results will be available by the year 2021 (projected end of the experimental program) [21].

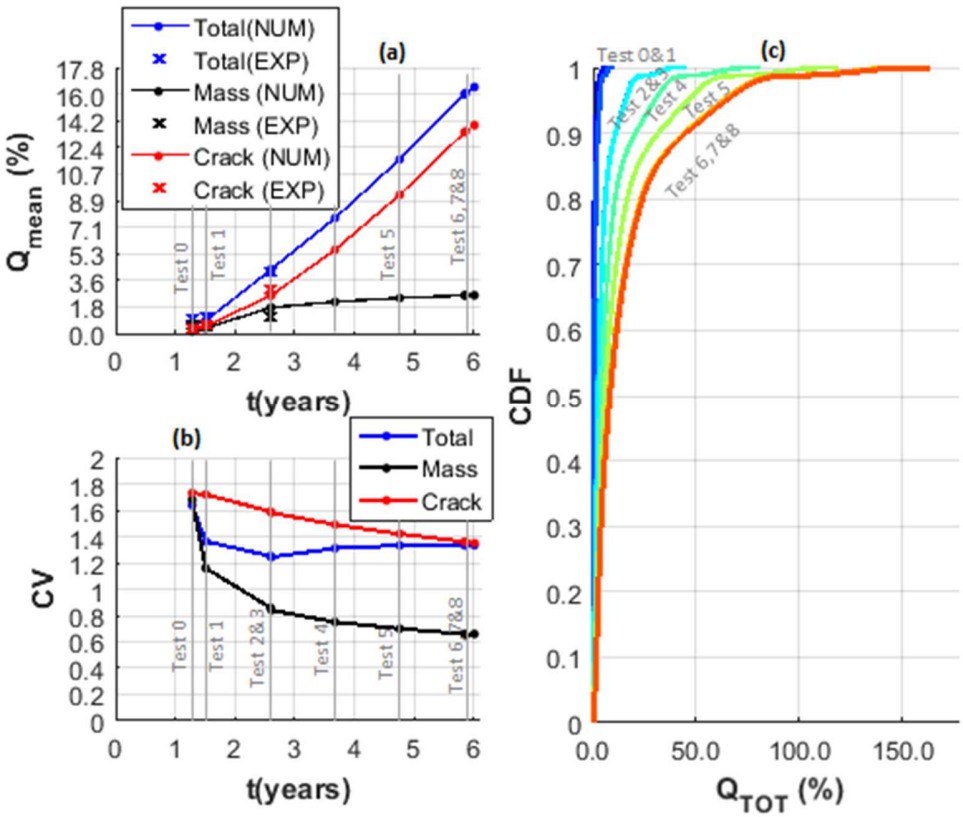

Fig. 13: Probabilistic description of the total and partial air leakage rates. Evolution in time of (a) the mean values; (b) the coefficient of variation and (c) the CDFs.

In a mean sense (Fig. 13a), the air flow rate through concrete mass is expected to evolve from 0.12% to 2.6% between the first and last pressurization tests and from 0.3% to 14% through the early age cracks. One can notice the adequacy of experimental values with the numerically predicted ones (for tests 0-3). The associated coefficient of variation (Fig. 13b) decreases over

time from 168% to 66%, from 173% to 135% and from 163% to 133% for the air through the mass, through the cracks and through the whole structure respectively. The resultant evolution of the associated CDF in time is depicted in Fig. 13c. A considerable increase in the leakage rates is observed between the 2nd and 3rd pressurization tests due to the increase of the inner operational temperature from 15°C (mean ambient temperature) to 35°C (thermo-activation effect).

As one can notice, and based on a deterministic analysis, the leakage rate is expected to exceed the default regulatory threshold of 10.1% after the 5th pressurization test (Test 4 in Fig. 13a) where the computed total air leakage rate is of 7.7% (the following value in is of 11.6% at the 6th test – Test 5 in Fig. 13a –). This means that maintenance and repair operations should be expected at this stage of the structure's operational phase to reinforce its tightness by filling cracks or covering its surface with impermeable substances. The leakage rate to overcome Q_{rep} is of 6.4% in order to allow a safe operational environment of the NCB until its projected 6-year operational lifespan (Fig. 14a). However, when accounting for the various THM-L uncertainties, the risk of exceeding the regulatory threshold becomes non null right after the 3rd pressurization test. As depicted in Fig. 14b, such risk increases over time up to 40% towards the 6-year period.

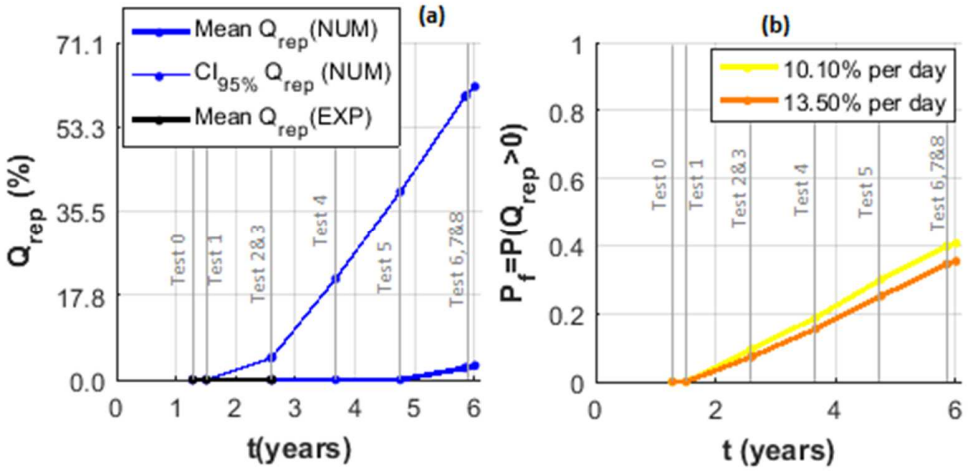

Fig. 14: Probabilistic description of the leakage rate exceeding the regulatory threshold. Evolution in time of (a) the mean value and (b) the risk of exceeding the regulatory threshold.

Based on such results, operators can define a reference probability of exceeding the leakage threshold and quantify the excess in order to allow preventive repair works and project a realistic evolution of their structures' performance in time.

Obviously, the reduction of such risk is conditioned by the control of uncertainties related to critical ageing phenomena identified previously (monitoring and control of the early age cracks, of the operational loads and of the transfer properties of concrete at the structural scale). The better and more precise those uncertainties are quantified, the more accurate and more reliable the risk of non-conformity in terms of the dry air leakage rate is estimated numerically.

5. Conclusions

In this contribution, a global stochastic THM-L approach is suggested to deal with the behaviour of large reinforced and prestressed structures under material and load related uncertainties. The developed 4-step strategy consists of (a) defining a physically admissible and representative staggered THM-L model; (b) the definition of its most influential parameters using a Hierarchized and Local Sensitivity Analysis both over time and through the chained calculation steps; (c) the identification of a PCE-based THM-L model and (d) the probabilistic and reliability analysis of the outputs of interest using CMCM at low cost.

Applied to the case of an experimental 1:3 scaled Containment Building, the following conclusions are retained:

- By using the HLSA, 9 most influential THM-L parameters (amongst more than 60 THM-L inputs) have been identified at low cost (up to 66% cost reduction compared to the case of a default LSA). They are all descriptive of critical physical ageing phenomena of concrete (drying, cracking, prestressing losses, transfer properties evolution in time).

- The qualitative results derived from the HLSA, in terms of the relative influence of each parameter/phenomenon, were confirmed by a GSA. This underlines the physical validity of HLSA though less accurate quantitatively in terms of variance estimation.
- The PCE development using the reduced list of most influential parameters led to a physically admissible and representative probabilistic description of THM-L quantities at a reasonable cost (tens of days only though deterministic calculations last for hours).
- Thanks to the suggested approach, the reliability analysis of the dry air leakage rate (which is a major indicator of the structural performance of NCBs) becomes straightforward within a reasonable time. This enhances the risk control of air leakage rate exceedance and allows a more conservative anticipation of repair and maintenance actions. As an example, and given the used uncertainties in the present work, it has been shown that the VeRCoRs structure might require repair and maintenance after 2-3 years of operations when uncertainties are accounted for; whereas deterministic approach predicts rather 4-5 years.
- Due to uncertainty propagation, leakage results are strongly affected by THM inputs variation. This underlines the importance of full THM-L probabilistic description rather than a partial one limited to one calculation step or one calculation phase. In particular, one can note that due to the physical coupling, uncertainties amplification is non-negligible and needs to be accounted for using full THM-L schemes.
- Finally, one can denote the general applicability of the stochastic THM-L approach in similar case studies (full scale NCBs, dams, reservoirs, etc.) and for different quantities of interest (temperature or strain or crack-opening or relative humidity based criteria for structural performance assessment).

6. On-going and future developments

In this work, the following issues have not been tackled but are considered for on-going and future developments:

- The used model is physically representative and is able to describe the structural response observed on site with reasonable accuracy. However, other phenomena could be of interest in such ageing structures with uncertainties both experimentally and numerically. For instance, there is (a) the effect of steel-concrete bond on the resulting cracking patterns [88] (b) the effect of cracking on the concrete's hydric diffusivity [89](c) the effect of self-healing in concrete on the evolution of early age crack's opening and ultimately on the leakage rate [90] (d) etc. These topics are considered out of the scope in the present work but are of interest within the VeRCoRs benchmark and within the forthcoming research efforts.
- Metamodelling cost optimization using adaptive schemes [91][92]: indeed, further cost reduction can be foreseen if such methods are applied. The main difficulty remains related to the definition of a physically admissible measuring precision at the structural scale. The quantification of such cost reduction vs. error limitation is forthcoming based on the present reference study.
- Model updating [93][94]: in usual cases, and due to the lack of data, predictive analyses lead to different results as the ones measured on site a posteriori. In such configurations, model updating is required to improve the model predictiveness based on the acquired data. The suggested approach can be used in that direction, to limit the number of parameters concerned by the updating and, accordingly, reduce the dimension of the inverse problem. This work is also set as forthcoming to the present contribution, as on-going Non Destructive Measuring of concrete properties' spatial variability is planned for the VeRCoRs mock-up as a part of a joint effort of the MACENA [95] and ENDE [24] projects.

Acknowledgements

This work was supported by EDF-SEPTEN/DTG/CIH within the Chair PERENITI agreement with the Grenoble INP Partnership Foundation and by the joint MACENA and ENDE project fund (ProjetIA-11-RSNR-0009 and ProjetIA-11-RSNR-0012). The author is grateful to EDF-SEPTEN for the provided in situ measurements. The Chair PERENITI partners shall not in any circumstances be deemed liable for the content of this publication which is only binding its author.

The 3SR lab is part of the LabEx Tec 21 (Investissements d'Avenir - Grant agreement n°ANR-11-LABX-0030).

Appendices

A. THM-L mode inputs and their associated distributions

A.1 Thermal inputs

Parameter			Deterministic analysis		HLSA			GSA / Probabilistic analysis		
			Ref.	Source	LB*	UB**	Source	CV	PDF	Source
1	Density	$\rho_c\left(\frac{ton}{m^3}\right)$	2.5	[21]	2.45	2.55	[21]			
2	Capacity	$C^p\left(\frac{kJ}{kg°K}\right)$	0.88		0.52	1.23	[6]	40 %	Log	Principle of maximum entropy [86]
3	Conductivity	$\lambda_c\left(\frac{J}{s\ m\ °K}\right)$	2.5	[18]	1.5	3.5				
4	Thermal effect on C^p	α_{C^p}	-0.0015		-0.0015	0				
5	Thermal effect on λ_c	α_λ	0.0016		0	0.0016				
6	Hydration effect on C^p	Yes or No	Yes		No	Yes				
7	Hydration effect on λ_c	Yes or No	Yes		No	Yes				
8	Activation energy	$E_a^{th}\left(\frac{kJ}{mo}\right)$	26		15.6	36.4				
9	Hydration heat	$Q_\infty\left(\frac{kJ}{m^3}\right)$	85	[21]	51	119		40 %	Log	Principle of maximum entropy [86]
10	Exchange coefficient	$h_{eq}^{th}\left(\frac{J}{m^2\ s\ °K}\right)$	10	[18]	6	14				
11	Operational temperature	$T_{ext}(°C)$	In situ	[21]	$0.6 * T_{ext}$	$1.4 * T_{ext}$				
12	Heating temperature at early age	$T_{ext}^{heat}(°C)$	$+30°C$		+18°C	+42°C				
-	Formwork thickness	$e_{cp}(mm)$	36							
-	Formwork conductivity	$\lambda_{cp}\left(\frac{J}{s\ m\ °K}\right)$	0.5							
-	Chemical affinity	$\dot{\alpha}$	Arctan							

*LB: Lower Bound **UB: Upper Bound

A.2 Hydric inputs

Parameter			Deterministic analysis		HLSA			GSA / Probabilistic analysis		
			Ref.	Source	LB*	UB**	Source	CV	PDF	Source
1	Initial water content	$C_{fw,0}\left(\frac{kg}{m^3}\right)$	132	[21]	105	158	[6]	20 %	Log	Principle of maximum entropy [86]
2	Diffusivity parameter	$A_w\left(\frac{10^{-12}\ m^2}{s}\right)$	3.1		2.5	3.7				
3	Diffusivity parameter	B_w	0.05		0.04	0.06		20 %	Log	Principle of maximum entropy [86]
4	Desorption parameter	a_w	7.6		6.1	9.1				
5	Desorption parameter	b_w	0.3		0.24	0.36				
6	Activation energy	$E_a^w\left(\frac{kJ}{mo}\right)$	39	[18]	31	47				
7	Mixing ratio	$r\left(\frac{g}{kg}\right)$	6.31	[21]	5	7.6				
8	External temperature	T_{ext}(°C)	In situ		$0.6 * T_{ext}$	$1.4 * T_{ext}$				
9	Exchange coefficient	$h_{eq}^w\left(\frac{10^{-9}\ m}{s}\right)$	3.4	[18]	2.7	4.1				
-	Voids content	φ_v (%)	14.6 %	[21]						
-	Initial cement content	$c\left(\frac{kg}{m^3}\right)$	320							

*LB: Lower Bound **UB: Upper Bound

A.3 Mechanical inputs

	Parameter			Deterministic analysis		HLSA			GSA / Probabilistic analysis		
				Ref.	Source	LB*	UB**	Source	CV	PDF	Source
1	Young's modulus		E(GPa)	36	[21]	32.4	39.6	[6]	10 %	Log	Empirical [21]
2	Hydration effect on E		b_E	0.81		0.4	1.2		[redacted]		
3	Structural tensile strength		R_t (MPa)	2.9	[18]	2.61	3.19		10 %	Log	Empirical [21]
4	Hydration effect on R_t		b_{R_t}	0.84	[21]	0.42	1.26		[redacted]		
5	Specimen tensile strength		$R_{t,ref}$ (MPa)	4.5		4.05	4.95				
6	Compressive strength		R_c(MPa)	48		43.2	52.8				
7	Hydration effect on R_c		b_{R_c}	0.74		0.37	1.11				
8	Fracture energy		$G_F\left(\frac{N}{m}\right)$	77		69.3	84.7				
9	Hydration effect on G_F		b_{G_F}	0.84		0.42	1.26				
10	Elastic Poisson ratio		ν_{ELAS}	0.2	[18]	0.1	0.3				
11	Burgers model parameters	Basic creep parameters	$k_{r,dev}^{BC}$ (GPa)	63	[21]	50.4	75.6				
12			$\eta_{r,dev}^{BC}$(GPa. s)	2.3 10^8		1.84 10^8	2.76 10^8				
13			$\eta_{i,dev}^{BC}$(GPa. s)	4.4 10^9		3.52 10^9	5.28 10^9				
14		Drying creep parameters	k_{dev}^{DC}(GPa)	2.5		2	3				
15			$\eta_{dev}^{DC}\left(\text{GPa}.\frac{s}{s}\right)$	9.1		7.28	10.92				
16		Reversible creep activation energy	$E_a^r\left(\frac{kJ}{mol}\right)$	25	[18]	20	30				
17		Irreversible creep activation energy	$E_a^i\left(\frac{kJ}{mol}\right)$	25		20	30				
18		Basic Poisson ratio	ν_{BC}	0.2	[25]	0.1	0.3				
19		Drying Poisson ratio	ν_{DC}	0.3		0.15	0.45				
20	Creep damage coupling		β_{coupl}	0.4	[18]	0.2	0.6				
21	Size effect	CV of E	CV_E	10 %	[21]	5 %	15 %				
22		Fluctuation length of E	l_{flu} (m)	1	[18]	0.5	1.5				
23		Autocorrelation function	ρ_{flu}	Gaussian	[6]	Exponential – Linear - Sinusoidal					
24		CV of R_t	CV_{R_t}	10 %	[21]	5 %	15 %				
25		Size effect scale length	D_c(m)	1	[18]	0.5	1.5				
26	Hydration percolation threshold		α_0	0.2		0.1	0.3				
27	Coefficient of Thermal Expansion		$\alpha_{TH}\left(\frac{\mu m}{m\,°C}\right)$	10		9	11		10 %	Log	Principle of maximum entropy [86]
28	Coefficient of endogenous shrinkage		$\alpha_{ES}\left(\frac{\mu m}{m}\right)$	74	[21]	66.6	81.4		10 %	Log	
29	Coefficient of drying shrinkage		$\alpha_{DS}\left(\frac{\frac{\mu m}{m}}{\frac{litre}{m^3}}\right)$	7.1		6.39	7.81		10 %	Log	

Parameter					Deterministic analysis		HLSA			GSA / Probabilistic analysis		
					Ref.	Source	LB*	UB**	Source	CV	PDF	Source
30	Prestressing	Gusset	Tangential	σ^{T}_{PREC} (MPa)	0.5	In situ measurements [21]	0.25	0.75	Considering 24 strain gauges [21]	50 %	Log	Empirical [21]
			Vertical	σ^{V}_{PREC}(MPa)	4.6		1.84	7.36				
		Wall	Tangential	σ^{T}_{PREC} (MPa)	9.0	Full scale 3D FE analysis of the VeRCoRs mock-up (validated by experimental observations for the wall and EAH)	4.95	13.05	Considering all nodes from each SV during the 3D FE analysis of the VeRCoRs mock-up (validated by experimental observations for the wall and EAH)			
			Vertical	σ^{V}_{PREC}(MPa)	6.0		4.50	7.50				
		EAH	Tangential	σ^{T}_{PREC} (MPa)	8.0		3.20	12.8				
			Vertical	σ^{V}_{PREC}(MPa)	6.4		1.92	10.88				
		Dome	Tangential	σ^{T}_{PREC} (MPa)	6.4		2.56	10.24				
			Vertical	σ^{V}_{PREC}(MPa)	1.8		0.09	3.51				
31	Pressurization	Gusset	Tangential	σ^{T}_{PRES} (MPa)	0.8	In situ measurements [21]	0.44	1.16	Considering 24 strain gauges [21]	50 %	Log	Empirical [21]
			Vertical	σ^{V}_{PRES}(MPa)	2.6		0.26	4.94				
		Wall	Tangential	σ^{T}_{PREC} (MPa)	6.0	Full scale 3D FE analysis of the VeRCoRs mock-up (validated by experimental observations for the wall and EAH)	3.42	8.58	Considering all nodes from each SV during the 3D FE analysis of the VeRCoRs mock-up (validated by experimental observations for the wall and EAH)			
			Vertical	σ^{V}_{PREC}(MPa)	3.5		2.59	4.41				
		EAH	Tangential	σ^{T}_{PRES} (MPa)	6.5		2.27	10.72				
			Vertical	σ^{V}_{PRES}(MPa)	2.9		0.43	05.36				
		Dome	Tangential	σ^{T}_{PREC} (MPa)	3.4		0.17	6.63				
			Vertical	σ^{V}_{PREC}(MPa)	0.9		-0.33	2.13				
-	FE characteristic length			h_{EF}(cm)	$4-8$	-						
-	Volume under tensile stresses for a split test			V_0(cm^3)	300	[55]						

*LB: Lower Bound **UB: Upper Bound

A.4 Leakage inputs

Parameter			Deterministic analysis		HLSA			GSA / Probabilistic analysis		
			Ref.	Source	LB*	UB**	Source	CV	PDF	Source
1	Permeability	$k_0 (10^{-17} m^2)$	2.71	[21]	1.35	4.06	[21]	50 %	Log	Empirical [21]
2	Klinkenberg coefficient	β_k (MPa)	0.18	[21]	0.09	0.27	Arbitrary expert's judgement considering the measurement of leakage parameters highly uncertain (CV of 50 % equal to the one of k_0). The actual CV is expected to be less than that.			
3	Saturation effect coefficient	c_d	0.46	[21]	0.23	0.69				
4	Damage effect coefficients	α'_d	11.3	[59]	5.65	16.95				
5		α_d	11.3		5.65	16.95				
6		β'_d	1.64		0.82	2.46				
7		β_d	1.64		0.82	2.46				
8	Roughness and shape coefficients	$\alpha_w \left(\frac{10^3}{m}\right)$	3.726	[62]	1.863	5.589				
9		β_w	1.19		0.6	1.8				
10	Matching law coefficient	δ	0.8	[16]	0.4	1.2				
11	Residual damage around a macrocrack	d_{lim}	0.2		0.1	0.3				
-	Intrados air pressure	$P_{air}^{intrados}$ (MPa)	0.52	[21]						
-	Extrados air pressure	$P_{air}^{extrados}$ (MPa)	0.10	[21]						

*LB: Lower Bound **UB: Upper Bound

B. Theoretical aspects of Polynomial Chaos Expansion and Collocation methods

B.1 General theoretical framework

Let's consider $\boldsymbol{\mathcal{M}}$ a computational model whose input parameters are represented by a random vector $\mathbf{X} = \{\mathbf{X_{1\leq i\leq N}}\}$. The model's random outputs $\mathbf{Y}$ verify $\mathbf{Y} = \{\mathbf{Y_{1\leq j\leq N'}}\} = \boldsymbol{\mathcal{M}}(\mathbf{X})$. Given the physical nature of our problem, $\mathbf{Y}$ is assumed to have a finite variance and can be fully defined using the following Hilbertian representation [63]:

$$\mathbf{Y} = \boldsymbol{\mathcal{M}}(\mathbf{X}) = \sum_{\mathbf{k=0}}^{+\infty} y_k \Psi_k(\mathbf{X}) \qquad \textbf{Eq. 18}$$

where $\{\Psi_{k\in\mathbb{N}}\}$ a numerable set of random variables forming the Hilbertian basis and $\{y_{k\in\mathbb{N}}\}$ are coordinates within that basis.

Several choices are possible for $\{\Psi_{k\in\mathbb{N}}\}$ verifying Eq. 18. Herein, a particular focus is granted to PCE in which the basis terms are multivariate orthonormal polynomials [96].The selection of the polynomial basis $\{P_{i\in\mathbb{N}}\}$ to be associated with each random parameter $X_i$depends on its marginal PDF $f_i(x_i)$. For instance, and under the hypothesis of independent random variables $\{X_i\}$, standard normal distributions $X_i \sim \aleph(0,1)$ lead to the use of Hermite polynomials $\{He_i\}$ and uniform distributions $X_i \sim U(-1,1)$ lead to the use of Legendre polynomials $\{Le_i\}$:

$$X_i \sim \aleph(0,1) \rightarrow \begin{cases} < P_m, P_n >_i = \int_{D_{X_i}} P_m(x)\ P_n(x)\, f_{X_i}(x)\ dx = \delta_{mn} \\ \{P_{k\in\mathbb{N}}\} = \left\{\frac{He_k}{\sqrt{k!}}\right\} \\ \begin{cases} He_{-1}(x) = He_0(x) = 1 \\ He_{k\geq 1}(x) = x\, He_{k-1}(x) - (k-1)\, He_{k-2}(x) \end{cases} \end{cases} \rightarrow \begin{cases} P_0(x) = 1 \\ P_1(x) = x \\ P_2(x) = \dfrac{x^2-1}{\sqrt{2}} \\ P_3(x) = \dfrac{x(x^2-3)}{\sqrt{6}} \end{cases}$$

$$X_i \sim U(-1,1) \rightarrow \begin{cases} < P_m, P_n >_i = \int_{D_{X_i}} P_m(x)\ P_n(x)\, f_{X_i}(x)\ dx = \delta_{mn} \\ \{P_{k\in\mathbb{N}}\} = \left\{\dfrac{Le_k}{\sqrt{\dfrac{1}{2k+1}}}\right\} \\ \left\{ Le_k = 2^k \sum_{i=0}^{k} x^i \binom{k}{i} \binom{\frac{k+i-1}{2}}{k} \right. \end{cases} \rightarrow \begin{cases} P_0(x) = 1 \\ P_1(x) = \sqrt{3}x \\ P_2(x) = \dfrac{\sqrt{5}}{2}(3x^2-1) \\ P_3(x) = \dfrac{\sqrt{7}}{2}x(5x^2-3) \end{cases} \qquad \textbf{Eq. 19}$$

where δ_{mn} the Kronecker symbol equal to 1 when n=m and 0 otherwise, D_{X_i} the support or definition domain of X_i.

As the random vector $\mathbf{X}$ contains N random variables, a multivariate polynomial construction is needed to express $\mathbf{Y}$ as shown in Eq. 18. It can be built up simply by product tensorization as following [63]:

$$\psi_{\alpha=\{\alpha_{1\leq i\leq N}\}}(\mathbf{x}) = \prod_{i=1}^{N} P_{\alpha_i}(x_i) \qquad \textbf{Eq. 20}$$

where $\{\psi_{\alpha=\{\alpha_{1\leq i\leq N}\}};\ \alpha_i\in\mathbb{N}\}$ a countable orthonormal basis to represent the random response $\mathbf{Y}$. $\alpha = \{\alpha_{1\leq i\leq N}\}$ a global index referring to the order of each polynomial α_i associated with the parameter's realization x_i.

Eq. 18 is an infinite sum. In practice, only a finite number of terms is to be retained for the PCE (truncated expression). Such number can be defined in a way so as not to exceed a certain polynomial degree $Q \leq \sum_{i=1}^{N} q_i$ with q_i the highest polynomial degree of the polynomial basis $\{P_{0\leq i\leq q_i}\}$ associated with each random input X_i:

$$\mathbf{Y} \approx \widehat{\mathbf{Y}} = \sum_{\sum \alpha_i = \mathbf{0}}^{\mathbf{Q}} y_\alpha \Psi_\alpha(\mathbf{X}) \qquad \textbf{Eq. 21}$$

Consequently, the number of terms in Eq. 21 should be $\binom{N+Q}{Q} = \frac{(N+Q)!}{N!Q!}$ which increases polynomially with N and Q (curse of dimensionality). As the required order Q for an accurate model approximation is not known a priori, conventional values around ~3 to 5 are considered in practice [85].

B.2 PCE coefficients identification

The identification of y_α coefficients in Eq. 21 requires several calls of the model. In the case of regression approaches [78], the number of calls should be higher than the number of unknowns for the problem to be well-posed: $N_{call} \geq \frac{(N+Q)!}{N!Q!}$. This however, does not take advantage of the orthonormality rule of the basis $\{\psi_{\alpha=\{\alpha_{1\leq i\leq N}\}}; \alpha_i \epsilon \mathbb{N}\}$ unlike projection methods where each coordinate y_α writes:

$$y_\alpha = \int_{D_X} \Psi_\alpha(\mathbf{x}) f_X(\mathbf{x}) \boldsymbol{\mathcal{M}}(\mathbf{x})\, d\mathbf{x} \qquad \textbf{Eq. 22}$$

with $f_X(\mathbf{x}) = \prod_{i=1}^{N} f_{X_i}(x_i)$ the joint PDF of the random vector **X.** The problem then is reduced to the evaluation of the previous integration using classical integration methods, in particular GQM:

$$y_\alpha \approx \sum_{j_1=1}^{S_1} \dots \sum_{j_N=1}^{S_N} w_{j_1}^1 \dots w_{j_N}^N \, \Psi_{\{\alpha_1,\dots,\alpha_N\}}(\mathbf{x_{1,j_1}}, \dots, \mathbf{x_{N,j_N}})\, \boldsymbol{\mathcal{M}}(\mathbf{x_{1,j_1}}, \dots, \mathbf{x_{N,j_N}}) \qquad \textbf{Eq. 23}$$

with $(x_{k,j_k};\ w_{j_k}^k)$ the integration points and the associated weights with respect to the distribution f_{X_k}. Compared to simulation methods where a relatively high number of random integration points is chosen (MCM or QMCM [97][98]), quadrature-based approaches [79][80] are preferred herein to limit the computational time. In that sense, it is worth recalling that, in the case of isotropic formulae, the GQM allows to integrate any polynomial function of a degree $2n-1$ with n suitable integration points. Consequently, for the PCE of an order Q and a polynomial basis with a maximum order q, the integrand in Eq. 22 has a maximal degree of Qq requiring $Qq+1$ integration points per parameter and $(Qq+1)^N$ calls of the model – if a full grid is retained –. For high number of inputs (more than ten inputs) such curse of dimensionality can be reduced by using adapted levels within the Smolyak quadrature scheme [91] or adaptive PCE methods [82].However such level is not known a priori and is defined based on a user-defined error threshold (only known if sufficient feedbacks are available for the problem of interest).

Herein, the default GQM is used. One can notice that there are two ways to truncate the PCE:

- Option1: Fixing the polynomial degrees for each parameter to a fixed value q. This would lead to a global degree of $Q = Nq$ in Eq. 21 (isotropic formulae). Using GQM, $(Nq^2+1)^N$ calls of the model need to be performed.
- Option 2: Fixing the global polynomial degree to a fixed value $Q = q$. The number of model calls is hugely reduced to $(q+1)^N$ as all terms y_α of which $\Psi_\alpha$verifies $\sum \alpha_i > Q$ are discarded.

Clearly, option 2 is less expensive than option 1 and is, therefore, retained herein. One is also reminded that, beyond accuracy issues, the higher q is the wider the covered domain of each random input X_i is (by definition a SR is only valid within its estimation domain). This aspect should be considered primarily (whether the scheme is adaptive or not) when selecting the q value to avoid extrapolation errors within the physically admissible variation domains.

B.3 Variance-based analysis

The influence of each input on the computed response can be estimated using GSA techniques. Particularly, Sobol' indexes [85] allow the decomposition of the output's variance into fractions that can be attributed to each input or set of inputs. Again, exploring the orthonormality rule, Sobol' indexes might be easily derived [83] after a convenient reordering of the PCE terms:

$$\begin{aligned}\hat{\mathbf{Y}}(\mathbf{x}) &= \sum_{\sum \alpha_i = \mathbf{0}}^{\mathbf{Q}} y_\alpha \Psi_\alpha(\mathbf{x}) \\ &= \mathbf{y_0} + \sum_{1\leq i_1\leq N} \sum_{\alpha\in\Gamma_{i_1}} y_\alpha \Psi_\alpha(\mathbf{x_{i_1}}) + \sum_{1\leq i_1<i_2\leq N} \sum_{\alpha\in\Gamma_{i_1,i_2}} y_\alpha \Psi_\alpha(\mathbf{x_{i_1}}, \mathbf{x_{i_2}}) + \cdots \\ &+ \sum_{1\leq i_1<\cdots<i_s\leq N} \sum_{\alpha\in\Gamma_{i_1,\dots,i_s}} y_\alpha \Psi_\alpha(\mathbf{x_{i_1}}, \dots, \mathbf{x_{i_s}}) + \cdots + \sum_{\alpha\in\Gamma_{1,\dots,N}} y_\alpha \Psi_\alpha(\mathbf{x_1}, \dots, \mathbf{x_N})\end{aligned} \qquad \textbf{Eq. 24}$$

with $y_0 = E[\hat{\mathbf{Y}}]$ the mean estimate of $\hat{\mathbf{Y}}$, $\Gamma_{i_1,\dots,i_s} = \left\{\alpha: \begin{matrix} \alpha_k > 0 & k \in (i_1,\dots,i_s) \\ \alpha_k = 0 & k \notin (i_1,\dots,i_s) \end{matrix}\right\}$ the set of α multi-indexes such that only the indexes $(i_1, \dots, i_s)$ are non-null.

The uniqueness of decomposition in Eq. 24 leads to the conclusion that it is exactly the Sobol' decomposition of $\hat{Y}$. This means that the s-ith Sobol' indexes are straightforward:

$$I^{PC}_{i_1,\dots,i_s} = \frac{\sum_{\boldsymbol{\alpha}\in\boldsymbol{\Gamma}_{i_1,\dots,i_s}} (y_\alpha)^2}{\sum_{\sum \alpha_i=1}^{Q} (y_\alpha)^2} \qquad \textbf{Eq. 25}$$

where $VAR[\hat{\mathbf{Y}}] = \sum_{\sum \alpha_i=0}^{Q} (y_\alpha)^2$. And so are the total Sobol indexes for each parameter X_i:

$$I^{PC}_{i} = \frac{\sum_{\mathbf{u}\in\mathbf{u}_i} (y_{\mathbf{u}})^2}{\sum_{\sum \alpha_i=1}^{Q} (y_\alpha)^2} \qquad \textbf{Eq. 26}$$

where $\mathbf{u_k} = \{\alpha: \alpha_k > 0\}$ the set of α multi-indexes such that the indice α_k is non-null.

Another alternative to computing Sobol' indexes is the DMCM [84][65]. This is particularly relevant when explicit model estimates are available but mostly when the PCE applicability is altered. Otherwise, the use of PCE-based GSA is recommended as it is considerably less time consuming (requiring less model calls compared to the DMCM).

Based on the ordering of I_i^{PC} terms, one might be led to identify some negligible indexes I_{i0}^{PC} compared to others. This informs about the negligible effect of the associated parameter X_{i0} variation over the domain $D_{X_{i0}}$ on the computed response variance. The NDP can therefore be reduced – a posteriori – to $(q+1)^{N' \leq N}$ where $N - N'$ is the number of identified non-influential parameters.

C. Instantaneous pre stressing losses according to the BPEL99 design code [99]

The formula suggested in the BPEL99 design code for instantaneous pre stressing losses is the following:

$$\frac{F(s)}{F_0} = \begin{cases} \left(1 - \frac{j}{j + r_m} \frac{5\,\rho_{1000}}{100} \frac{F_0 e^{f(\alpha - 2\alpha_d) + \varphi(s - 2\,s_d)} - \mu_0\, S_a\, \sigma_y}{S_a\, \sigma_y}\right) e^{f(\alpha - 2\,\alpha_d) + \varphi(s - 2\,s_d)} & \text{for } s \leq d \\ e^{-f\alpha - \varphi s} - \left(\frac{j}{j + r_m} \frac{5\,\rho_{1000}}{100} \frac{F_0 e^{f(\alpha - 2\,\alpha_d) + \varphi(s - 2\,s_d)} - \mu_0\, S_a\, \sigma_y}{S_a\, \sigma_y}\right) e^{f(\alpha - 2\alpha_d) + \varphi(s - 2\,s_d)} & \text{for } s \geq d \end{cases} \qquad \textbf{Eq. 27}$$

$$d \text{ verifies } \frac{E_a S_a \Delta}{F_0} = \int_0^d \left(e^{-f\alpha - \varphi s} - e^{f(\alpha - 2\,\alpha_d) + \varphi(s - 2\,s_d)}\right) ds$$

With:

- F(s) is the effective tension in cables at a given curvilinear abscissa s
- F_0 is the initial applied tension in cables
- $S_a$is the cable's cross section
- σ_y is the steel yielding strength
- f is the angular friction coefficient representing losses due to angular frictions
- φ is the linear friction coefficient representing losses due to linear frictions
- α is the deviation angle
- Δ is the anchorage decline and d is the domain where prestressing losses due to this decline are active. At this position: $\alpha = \alpha_d$ and $s = s_d$
- $r_m = S_b/P_b$ is the ratio of the concrete surface to its perimeter
- j a given time value for which the prestressing losses are forseen (in days). The ratio $\frac{j}{j+r_m}$ tends rapidly towards 1 for the long term phase.
- ρ_{1000} is the relaxation of steel cables at 1000 hours (in %)
- μ_0 is a steel relaxation coefficient

In this work, the used values are the following: $\rho_{1000} = 2.5\%$, $f = 0.17\ rad^{-1}$, $\varphi = 0.0015\ m^{-1}$, $\mu_0 = 0.43$, $\sigma_y = 1488$ MPa, $E_a = 190\ GPa$, $\Delta = 8$ mm, j=2557 days.

References

[1] Jason L., Pijaudier-Cabot G., Ghavamian S., Huerta A. Hydraulic behavior of a representative structural volume for containment buildings. Nuc. Eng. Des. 2007. 237(12-13): 1259-1274. DOI: https://doi.org/10.1016/j.nucengdes.2006.09.035
[2] Asali M., Capra B., Mazars J., Colliat J.B. Numerical Strategy for forecasting the leakage rate of inner contnaimens in double-wall nuclear reactor buildings. Adv. Conc. Tech. 2016. 14: 408-420 DOI: http://dx.doi.org/10.3151/jact.14.408
[3] Niklasch C., Herrmann N. Non-linear fluid-structure interaction calculation of the leakage behaviour of cracked concrete walls. 2009. Nuc. Eng. Des. 239(9): 1628-1640. DOI: http://dx.doi.org/10.1016/j.nucengdes.2008.09.001
[4] Jason L., Masson B. Comparison between continuous and localized methods to evaluate the flow rate through containment concrete structures. Nuclear engineering and design 2014 277: 146-153 DOI: https://doi.org/10.1016/j.nucengdes.2014.06.010
[5] Bouhjiti D. E.-M., Boucher M., Briffaut M., Dufour F., Baroth J., Masson B. Accounting for realistic Thermo-Hydro-Mechanical boundary whilst modeling the ageing of concrete in nuclear containment buildings: Model validation and sensitivity analysis. Eng. Struct. 2018. 166: 314-338. DOI: https://doi.org/10.1016/j.engstruct.2018.03.015
[6] Bouhjiti D. E.-M., Blasone M. C., Baroth J., Dufour F., Masson B., Michel-Ponnelle S. Statistical modelling of cracking in large concrete structures under Thermo-Hydro-Mechanical loads: Application to Nuclear Containment Buildings. Part 2: Sensitivity analysis. Nuc. Eng. Des. 2018. 334(1) : 1-23. DOI : https://doi.org/10.1016/j.nucengdes.2018.04.013
[7] Ulm F.-J., Coussy O. Couplings in early-age concrete: From material modeling to structural design. International Journal of Solids and Structures 1998 35(31):4295-4311 DOI: http://dx.doi.org/10.1016/S0020-7683(97)00317-X
[8] Mensi R., Acker P., Attolou A. Séchage du béton : analyse et modélisation. Materials and structures 1988 21(3): 3-12 DOI : http://dx.doi.org/10.1007/BF02472523
[9] Wittmann F.H., Roelfstra P. Total deformation of loaded drying creep. Cement and Concrete Research 1980 10(5):601-610 DOI: http://dx.doi.org/10.1016/0008-8846(80)90023-X
[10] Bažant Z.P., Chern J.C. Concrete creep at variable humidity: Constituve law and mechanisms. Materials and Structures. 1985 18(103): 01-20 DOI: http://dx.doi.org/10.1007/BF02473360
[11] Sellier A., Multon S., Buffo-Lacarrière L., Vidal T., Bourbon X., Camps G. Concrete creep modelling for structural applications: non-linearity, multi-axiality, hydration, temperature and drying effects. 2016. 79: 301-315. DOI: http://dx.doi.org/10.1016/j.cemconres.2015.10.001
[12] Bažant Z.P. Size effect on structural strength: a review. Archive of applied mechanics 1999 69(9): 703-725 DOI: http://dx.doi.org/10.1007/s00419005025
[13] Alarcon-Ruiz L., Brocato M., Dal Pont S., Feraille A. Size effect in concrete Intrinsic Permeability Measurements. Transp Porous Med. 2010. 85: 541-564. DOI: http://dx.doi.org/10.1007/s11242-010-9577-9.
[14] Mazars, J., Hamon, F., Grange, S. A new 3D damage model for concrete under monotonic, cyclic and dynamic loadings. Materials and structures 2015 48(11): 3779-3793 DOI: https://doi.org/10.1617/s11527-014-0439-8
[15] Giry C., Dufour F., Mazars J. Stress based nonlocal damage model. International Journal of Solids and Structures 2011 48(25-26): 3431-3443 DOI: http://dx.doi.org/10.1016/j.ijsolstr.2011.08.012
[16] Bouhjiti D. E.-M., Ezzedine El Dandachy M., Dufour F., Dal Pont S., Briffaut M., Baroth J., Masson B. New continuous strain-based description of concrete's damage-permeability coupling. Num. Anal. Meth. In Geomech. 2018. 42(14): 1671-1697. DOI: https://doi.org/10.1002/nag.2808
[17] Gawin D., Pesavento F., Schrefler B. A simulation of damage-permeability coupling in hydro-thermo-mechanical analysis of concrete at high temperature. Communication in numerical methods in engineering 2002 18(2): 113–119 DOI: https://doi.org/10.1002/cnm.472
[18]Bouhjiti D. E.-M., Baroth J., Briffaut M., Dufour F., Masson B. Statistical modelling of cracking in large concrete structures under Thermo-Hydro-Mechanical loads: Application to Nuclear Containment Buildings. Part 1: Random Field effects (reference analysis). Nuc. Eng. Des. 2018. 333: 196-223. DOI : https://doi.org/10.1016/j.nucengdes.2018.04.005
[19] Bouhjiti D. E.-M., Baroth J., Dufour F., Masson B. Prediction of air permeability in large RC structures using a stochastic FE THM modeling strategy. *Proceedings of the Conference on Computatioanl modeling of concrete and concrete structures (Euro-C).* 2018. Bad Hofgastein, Austria.
[20] Li et al. 1993 Li C., Der Kiureghian A., Ke J.B. (1993). Optimal discretization of random fields. Engineering mechanics. 119(6): 1136-1154. DOI: http://dx.doi.org/10.1061/(ASCE)0733-9399(1993)119:6(1136)
[21] VeRCoRs project description and data available at: https://fr.xing-events.com/OLD-EDF-vercors-project.html / https://www.conference-service.com/EDF-VeRCoRs-Benchmark-2018/welcome.cgi
[22] CEOS project: https://www.ceosfr.irex.asso.fr/en/
[23] EvaDéOS project: https://agence-natioanle-recherche.fr/en/anr-funded-project/?tx_lwmsuivibilan_pi2[CODE]=ANR-11-VILD-0002
[24] ENDE project: https://agence-natioanle-recherche.fr/ProjetIA-11-RSNR-0009

[25] Charpin L., Le Pape Y., Coustabeau E., Masson B. EDF Study of 10-Year Concrete Creep under Unidirectional and Biaxial Loading: Evolution of the Poisson Coefficient under Sealed and Unsealed Conditions. 2015. ASCE-10th International Conference on Mechanics and Physics of Creep, Shrinkage, and Durability of Concrete and Concrete Structures
[26] Le Roy R., Le Maou F., Torrenti J.M. Long term basic creep behavior of high performance concrete: data and modeling. 2017. Mater. And Struc. 50: 85. DOI: https://doi.org/10.1617/s11527-016-0948-8
[27] Gaspar A., Lopez-Caballero F., Modaressi-Farahmand-Ravazi A., Gomes-Correia A. Methodology for a probabilistic analysis of an RCC gravity dam construction. Modelling of temperature, hydration degree and ageing degree fields. 2014. Eng. Struct. 65: 99-110. DOI: https://doi.org/10.1016/j.engstruct.2014.02.002
[28] Göbel L., Lahmer T., Osburg A. Uncertainty analysis in multiscale modeling of concrete based on continuum micromechanics. 2017. J. of Mechanics. 65: 14-29. DOI: https://doi.org/10.1016/j.euromechsol.2017.02.008
[29] Kwon S.J., Na U.J., Park S.S., Jung S.H. Service life prediction of concrete wharves with early-aged crack: Probabilistic approach for chloride diffusion. 2009. Structural Safety. 31(1): 75-83. DOI: https://doi.org/10.1016/j.strusafe.2008.03.004
[30] Conciatori D., Grégoire E., Samson E., Marchand J., Chouinard L. Statistical analysis of concrete transport properties. 2014. Materials and Structures. 47(1-2): 89-103. DOI: https://doi.org/10.1617/s11527-013-0047-z
[31] Issaadi N., Nouviaire A., Belarbi R., Aït-Mokhtar A., Moisture characterization of cementitious material properties: Assessment of water vapor sorption isotherm and permeability variation with ages. 2015. Construction and Building Materials 83: 237–247. DOI: https://doi.org/10.1016/j.conbuildmat.2015.03.030
[32] Issaadi N. 2015. Effects de la variabilité des propriétés de matériaux cimentaires sur les transferts hygrothermiques : développement d'une approche probabiliste. *PhD Thesis [in French]. Univ. De La Rochelle. France*
[33] Balomenos G. P., Pandey M. D. Probabilistic FE investigation of pre stressing loss in nuclear containment wall segments. 2017. Nuc. Eng. Des. 311: 50-59. DOI: https://doi.org/10.1016/j.nucengdes.2016.11.018
[34] Jin S.S., Cha S.-L., Jung H.-J. Improvement of concrete creep prediction with probabilistic forecasting method under model uncertainty. Construct. Build. Mater. 2018. 184: 617-633. DOI: https://doi.org/10.1016/j.conbuildmat.2018.06.238
[35] Berveiller M., Le Pape Y., Sudret B., Perrin F. Bayesian updating of long –term creep strains in concrete containment vessels using a non-intrusive stochastic finite element method. Int. Conf. Applications of statistics and Probability in Civil Engineering, ICASP'10 2007 Tokyo, Japan
[36] Han B., Xiang T.-Y., Xie H-B. A Bayesian inference framework for predicting the long-term deflection of concrete structures caused by creep and shrinkage. 2017. Eng. Structu. 142: 46-55. DOI: https://doi.org/10.1016/j.engstruct.2017.03.055
[37] Tailhan J.-L., Rossi P., Caucci A. M. Probabilistic modeling of cracking in concrete. 2014. EJCE. 18(7-8): 770-779. DOI: https://doi.org/10.1080/19648189.2013.878256
[38] Dameron R.A., Rashid Y.R., Tang H.T. Leak area and leakage rate prediction for probabilistic risk assessment of concrete containments under severe core conditions. 1995. Nucl. Eng. Des. 156: 173-179. DOI: https://doi.org/10.1016/0029-5493(94)00943-S
[39] Tang H.T., Dameron R.A., Rashid Y.R. Probabilistic evaluation of concrete containment capacity for beyond design basis internal pressures. 1995. 157: 455-467. DOI: https://doi.org/10.1016/0029-5493(95)01014-9
[40] Conceição J., Faria R., Azenha M., Mamede F., Souza F. (2014). Early-age behaviour of the concrete surrounding a turbine spiral case: Monitoring and thermo-mechanical modeling. Engineering structures. 81:327-340. DOI: https://doi.org/10.1016/j.engstruct.2014.10.009
[41] Briffaut M., Benboudjema F., Torrenti J.-M., Nahas G. (2011). Numerical analysis of the thermal active restrained shrinkage ring test to study the early age behavior of massive concrete structures. Engineering Structures. 33(4): 1390-1401. DOI: https://doi.org/10.1016/j.engstruct.2010.12.044
[42] Buffo-Lacarrière L., Sellier A., Kolani B. (2014). Application of thermohydro-chemo-mechanical model for early age behaviour of concrete to experimental massive reinforced structures with strain–restraining system. European Journal of Environmental and Civil Engineering. 18(7): 814-827. DOI: https://doi.org/10.1080/19648189.2014.896754
[43] Powers T. C., Brownyard T. L. (1946). Studies of the physical properties of hardened Portland cement of paste. ACI proc. 43(9): 469-504.
[44] Mensi R., Acker P., Attolou A. Séchage du béton : analyse et modélisation. Materials and structures 1988 21(3): 3-12 DOI : http://dx.doi.org/10.1007/BF02472523
[45] Bažant Z.P., Kristek V., Vitek J.L. (1992). Drying and cracking in box-girder bridge segment. Journal of Structural Engineering 1992 118(1): 305-321 DOI: http://dx.doi.org/10.1061/(ASCE)0733-9445(1992)118:1(305)
[46] Thiery M., Baroghel-Bouny V., Bourneton N., Villain G., Stefani C. Modélisation du séchage des bétons. Analyse des différents modes de transfert hydrique. Revue Européenne de Génie Civil 2007 11: 541-577.
[47] De Schutter G., Taerwe L. Degree of hydration-based description of mechanical properties of early age concrete. Materials and structures 1996 29(6): 335-344 DOI: http://dx.doi.org/10.1007/BF02486341

[48] De Schutter G. Degree of hydration based kelvin model for the basic creep of early age concrete. Materials and Structures 1999 30(4): 260-265 DOI: http://dx.doi.org/10.1007/BF02479595
[49] Bažant Z.P. Thermodynamics of interacting continua with surfaces and creep analysis of concrete structures. Nuclear Engineering and Design 1972 20(2): 477-505 DOI: http://dx.doi.org/10.1016/0029-5493(72)90124-0
[50] Mazars, J., Hamon, F., Grange, S. A new 3D damage model for concrete under monotonic, cyclic and dynamic loadings. Materials and structures 2015 48(11): 3779-3793 DOI: https://doi.org/10.1617/s11527-014-0439-8
[51] Hillerborg A. Application of fracture mechanics to concrete – Summary of a series of lectures. 1988 Lund Institute of Technology.
[52] Mazzotti C., Savoia M. Nonlinear creep damage model for concrete under uni axial compression. Journal of engineering mechanics 2003 129(9): 1065 – 1075 DOI: http://dx.doi.org/10.1061/(ASCE)0733-9399(2003)129:9(1065)
[53] Torrenti J.M., Nguyen V. H., Colina H., Le Maou F., Benboudjema F., Deleruyelle F. Coupling between leaching and creep of concrete. Cement and concrete research 2008 38(6): 816 – 821 DOI: http://dx.doi.org/10.1016/j.cemconres.2008.01.012
[54] Sciumè G., Benboudjema F. A viscoelastic unitary crack opening strain tensor for crack width assessment in fractured concrete structures. Mech Time-Depend Mater 2017 21:223-243 DOI: http://dx.doi.org/10.1007/s11043-016-9327-7
[55] Sellier A., Millard A. Weakest link and localization WL²: a method to conciliate probabilistic and energetic scale effects in numerical models. European Journal of Environmental and Civil Engineering 2014 18(10): 1177-1191 DOI: http://dx.doi.org/10.1080/19648189.2014.906368
[56] Ghanem, R., Spanos, P. Stochastic finite elements – A spectral approach. Revised edition. Dover Publications, INC. New York. USA, 1991.
[57] Li et al. 1993 Li C., Der Kiureghian A., Ke J.B. (1993). Optimal discretization of random fields. Engineering mechanics. 119(6): 1136-1154. DOI: http://dx.doi.org/10.1061/(ASCE)0733-9399(1993)119:6(1136)
[58] Picandet V., Khelidj A., Bastian G. Effect of axial compressive damage on gas permeability of ordinary and high performance concrete. Cement and Concrete research 2001 31(11): 1525-1532 DOI: https://doi.org/10.1016/S0008-8846(01)00546-4
[59] Choinska M., Khelidj A., Chatzigeorgiou G., Pijaudier-Cabot G. Effects and interactions of temperature and stress-level related damage on permeability of concrete. Cement and Concrete research 2007 37(1): 79-88 DOI: https://doi.org/10.1016/j.cemconres.2006.09.015
[60] Verdier J. Contribution à la caractérisation de l'évolution du taux de fuite des enceintes de confinement du parc nucléaire. 2001. Thesis [in french] Univ. Toulouse Paul Sabatier 3. France
[61] Abbas A., Carcasses M., Ollivier J.-P. 1999. Gas permeability of concrete in relation to its degree of saturation. Materials and structures. 32(1): 3-8. DOI: https://doi.org/10.1007/BF02480405
[62] Rastiello G., Tailhan J. L., Rossi P. Dal Pont S. Macroscopic probabilistic cracking approach for the numerical modeling of fluid leakage in concrete. Annals of Solid and Structural Mechanics 2015 7(1): 1-16 DOI: https://doi.org/10.1007/s12356-015-0038-6
[63] Soize, C. and R. Ghanem (2004). Physical systems with random uncertainties: chaos representations with arbitrary probability measure. SIAM J. Sci. Comput. 26 (2), 395– 410. DOI: https://doi.org/10.1137/S1064827503424505
[64] Xiu, D. and G. Karniadakis (2002). The Wiener-Askey polynomial chaos for stochastic differential equations. SIAM J. Sci. Comput. 24 (2), 619–644. DOI: https://doi.org/10.1137/S1064827501387826
[65] A.Saltelli, M. Ratto, T. Andres, F. Campolongo, J. Cariboni, D. Gatelli, M. Saisana, S. Tarantola. Global Sensitivity Analysis: The Primer. WILEY/MATHEMATICS & STATISTICS/APPLIED PROBABILITY & STATISTICS/MODELS 2018 Chapter II: 53-108
[66] Cotter S. C. A screening design for factorial experiments with interactions. Biometrika 1979 66(2): 317-320 DOI: https://doi.org/10.1093/biomet/66.2.317
[67] Cornell A.C. (1971). First Order uncertainty analysis of soils deformation and stability. Proc, 1st conf. on Applications of Statistics and Probability to Soil and Structural Engineering: 130–144
[68] Rosenblueth E. (1975). Point estimates for probability moments. Proc, Nat. Acad. Sciences. 72 :3812–3814
[69] Yamazaki F., Shinozuka M., Dasgupta G. Neumann expansion for stochastic finite element analysis. Eng. Mech. 1988 114(8) :1335–1354. DOI: https://doi.org/10.1061/(ASCE)0733-9399(1988)114:8(1335)
[70] Deodatis G. Weighted integral method. I: stochastic stiffness matrix. Eng. Mech. 1991. 117(8): 1851-1864. DOI: https://doi.org/10.1061/(ASCE)0733-9399(1991)117:8(1851)
[71] Xianggui Q., Wu C. F. J. (2005). One factor at a time designs of resolution V. Statistical planning and inference. 2005. Statistical Planning and Inference. 131:407-416. DOI: https://doi.org/10.1016/j.jspi.2004.03.002
[72] Cavazzuti M. (2012). Optimization methods: from theory to design of scientific and technological aspects in mechanics. Springer science & business media
[73] Montgomery D. (2012). Design and analysis of experiments. John Wiley and sons. New York. USA
[74] Wu C. F. J., Hamada M. (2000). Experiments: Planning, Analysis and Parameter Design Optimization. Wiley, New York. USA
[75] Daniel C. One-at-a-time plans. 1973. Amer. Statist. Assoc. 68: 353–360. DOI: https://doi.org/10.2307/2284076

[76] Morris M. D. Factorial sampling plans for preliminary computational experiments. 1991. Technometrics. 33:161-174. DOI: https://doi.org/10.2307/1269043
[77] Sobol', I.M. (1993). Sensitivity estimates for nonlinear mathematical models. 1993. Math. Model. Comput. Exp., 1: 407–417. John Wiley and Sons, Inc.
[78] Berveiller M., Sudret B., Lemaire M. Stochastic Finite element : a non-intrusive approach by regression. 2006. Comput. Mech. 15(1-3): 81-92. DOI: https://doi.org/10.3166/remn.15.81-92
[79] Baroth J., Bodé L., Bressolette P., Fogli M. SFEM using Hermite Polynomials: an approach for solving nonlinear problems with uncertain parameters. 2006. Comp. Meth. Appl. Mech. 195:6479-6501. DOI: https://doi.org/10.1016/j.cma.2007.04.017
[80] Baroth J., Bressolette P., Chauviere C., Fogli M. An efficient SFEM using Lagrange Polynomials: application to nonlinear mechanical problems with uncertain parameters. 2007. Comp. Meth. Appl. Mech. 196(46-58): 4419-4429. DOI: https://doi.org/10.1016/j.cma.2007.04.017
[81] Gary W. G., Dong Z., Aitchison P. Adaptive Response Surface Method – A global optimization scheme for computation-intensive design problems. 2001. Eng. Optim. 3(6): 707-734. DOI: https://doi.org/10.1080/03052150108940940
[82] Blatman G., Sudret B. An adaptive algorithm to build up sparse polynomial chaos expansions for stochastic FE analysis. Prob. Eng. Mech. 2010 25(2): 183-197 DOI: https://doi.org/10.1016/j.probengmech.2009.10.003
[83] Sudret B. Global Sensitivity analysis using polynomial chaos expansions. Reliab. Eng. Safety 2008 93(7):964-979 DOI: https://doi.org/10.1016/j.ress.2007.04.002
[84] Sobol' I.M. Global sensitivity indices for nonlinear mathematical models and their Monte Carlo estimates. Mathematica and computers in simulation 2001 55(1-3):271-280. DOI: https://doi.org/10.1016/S0378-4754(00)00270-6
[85] Baroth J., Breysse D., Schoefs F. Construction Reliability: Safety, Variability and Sustainability. 2011. Wiley-ISTE. ISBN: 978-1-84821-230-5.
[86] Jaynes E. T. Information Theory and Statistical Mechanics. 1957. The physical review. 106(4): 620-60. DOI: https://doi.org/10.1103/PhysRev.106.620
[87] Courtois A., Henault J.-M., Simon A., Beck Y.-L., Salin J. La surveillance en exploitation des enceintes de confinement et des aéroréfrigérants à tirage naturel du parc nucléaire d'EDF. 2011. Revue Générale Nucléaire. 2 : 49-59.
[88] Michou A., Hilaire A., Benboudjema F., Nahas G., Wyniecki P., Berthaud Y. Reinforcement–concrete bond behavior: Experimentation in drying conditions and meso-scale modeling. 2015. Engineering Structures. 101: 570-582. DOI: https://doi.org/10.1016/j.engstruct.2015.07.028
[89] Bažant Z.P., Sener S., Kim J.-K. Effect of cracking on drying permeability and diffusivity of concrete. 1987. ACI materials Journal. 84(5): 351-357.
[90] Zemann M., Hermann N., Dehn F. Calcite formation on steamed concrete surfaces and its potential for sealing cracks. 2019. Construction and Building Materials. 203: 1-8. DOI: https://doi.org/10.1016/j.conbuildmat.2019.01.091
[91] Smolyak S. Quadrature and interpolation formulas for tensor products of certain classes of functions. 1963. Soviet. Math. Dokl. 4 :420-243.
[92] Blatman G., Sudret B. (2011). Adaptive sparse polynomial chaos expansion based on least angle regression. Computational physics. 230(6): 2345-2367. DOI: https://doi.org/10.1016/j.jcp.2010.12.021
[93] Berveiller M., Le Pape Y., Bruno S. Updating the long-term creep strains in concrete containment vessels by using Markov chain Monte Carlo simulation and polynomial chaos expansions. 2012. Structure and Infrastructure Engineering. 8(5): 425-440. DOI: https://doi.org/10.1080/15732479.2010.539057
[94] Zhang R., Mahadevan S. (2000). Model uncertainty and Bayesian updating in reliability-based inspection. Structural safety. 22(2): 145-160. DOI: https://doi.org/10.1016/S0167-4730(00)00005-9
[95] MACENA project: https://anr.fr/ProjetIA-11-RSNR-0012
[96] Xiu, D. and G. Karniadakis (2002). The Wiener-Askey polynomial chaos for stochastic differential equations. SIAM J. Sci. Comput. 24 (2), 619–644. DOI: https://doi.org/10.1137/S1064827501387826
[97] McKay M. D., Beckman R. J., Conover W. J. A comparison of three methods for selecting values of input variables in the analysis of output from a computer code. Technometrics 1979
[98] Blatman G., Sudret B., Berveiller M. Quasi-random numbers in stochastic FE analysis. Mécaniques & industries 2007 8(3) : 289-297 DOI : https://doi.org/10.1051/meca:2007051
[99] Règles techniques de conception et de calcul des ouvrages en béton précontraint suivant la méthode des états limites. BPEL 91 revised 99.